

## Response to reviewer comments for manuscript: “On the calibration of FIGAERO-ToF-CIMS: importance and impact of calibrant delivery for the particle phase calibration”

Ylisirniö et al.,

We thank the reviewer for his/her constructive comments regarding our paper. Below we will address the specific issues point by point. The reviewer’s comments are in black and our answers are in blue. Changes to the Manuscript or Supplement Information are highlighted in red. Line numbers before the red response text refer to line numbers in the modified manuscript.

### Additional changes by authors:

We added additional discussion about potential effect of collected aerosol mass loading to Section 3.3.

Line 281:

“An additional aspect that has been reported to shift  $T_{max}$  values is the amount of collected aerosol mass on the PTFE filter (Huang et al., 2018), becoming important when collected particulate mass is around several micrograms. We tested the mass loading effect by collecting different amounts of atomized PEG’s up to 200 ng of mass and found no clear difference between measured  $T_{max}$  values (data not shown). However, as collected aerosol mass on the FIGAERO filter can easily reach microgram amounts, especially when sampling in highly polluted environments and as we did not rigorously test how  $T_{max}$  values behave above 200 ng, we suggest that this effect is investigated further in future publications.”

### Reviewer 1:

#### General comments:

1) Dependence on the solution concentration. The authors demonstrate that by adjusting the diameter in the evaporation model, they can reproduce the results for different solution concentrations. In order to have this in line with the subsequent reasoning about the SEM image, they should show different SEM images with different solution concentrations showing that indeed smaller structures are deposited on the filter in the case of lower solution concentrations. If the diameter really controls this behavior, also a calibration with the atomizer and particles around 1  $\mu\text{m}$  could support this.

The reviewer makes a good point regarding the additional SEM figures with different solution concentrations. Below is a SEM figure showing deposition using a solution of  $0.25 \text{ g L}^{-1}$  which is a much higher concentration than the  $0.01 \text{ g L}^{-1}$  used in Fig. 5b) of the manuscript. Careful analysis

may reveal some differences between the “ring structures” in these two cases. But, in our opinion, it is almost impossible to do a quantitative analysis of the true size and mass of the evaporating unit from the filter based solely on this type of SEM pictures. While it is easy to measure the diameter and width of the “ring”, we have no information about the thickness of the layer. Additionally, part of the deposited compound/mass may be hiding inside the filter and cannot be seen with this method.

Thus, it is our understanding that a more thorough analysis using a higher number of different solution concentrations would not lead to more relevant information. We will continue to just use the SEM pictures to qualitatively verify that the two deposition methods (syringe vs atomization) lead to very different structures of the deposited material on the filter which impact the evaporation behaviour. However, we will more strongly emphasise the qualitative nature of the SEM pictures in the modified manuscript.

Line 242:

“We want to emphasize that as SEM cannot distinguish deposited material situated inside the filter or measure the layer depth, the images shown here should be considered only as qualitative evidence.”

Unfortunately, creating monodisperse particles in the range of 1  $\mu\text{m}$  is not trivial with our equipment. Optimising the particle generation and size selection for that size range was outside of the scope of this study.

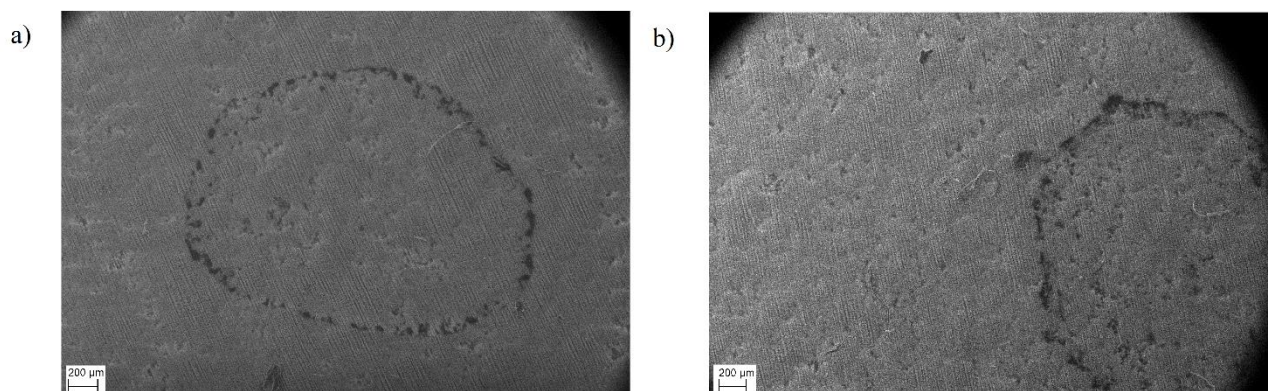


Figure 1. Panel a) Shows Fig.5 b) from manuscript showing 3  $\mu\text{l}$  of PEG-8 with concentration of 0.01  $\text{g L}^{-1}$ . Panel b) shows SEM figure of 3  $\mu\text{l}$  of PEG-8 with concentration of 0.25  $\text{g/l}$  in ACN deposited on the filter.

2) The authors base their reasoning mainly on the SEM images of the FIGAERO filter for the atomization method and the syringe method. However, they only show SEM pictures for one substance. While I don't doubt their conclusion, other SEM images should be added. The authors make the statement that the vacuum in the SEM could evaporate all the other substances than PEG-8, but how can they then conclude that it is not the SEM sample preparation (i.e. bringing the filter into a vacuum), which causes the structures observed on the filter?

We argue that the formation of the ring structure is caused by the evaporation of the initially deposited droplet, i.e., the evaporation of the solvent, ACN. Changing the rate of evaporation (i.e., by evaporating at ambient or SEM pressure) may change the exact size and shape of the “ring

structure”, but the structure will still be formed and be very different from the same mass deposited as sub-micron particles.

The only difference between normal FIGAERO sample treatment and SEM sample treatment is that SEM is operated in vacuum while in the FIGAERO the samples are not exposed to lowered pressures. PEG-8 was selected for the screening due to its low vapour pressures, to minimise the likelihood of any evaporation of the example calibration compound in the vacuum of the SEM which might skew the results from the SEM. While it is possible to use some solid compound like citric acid, which would not easily evaporate from the filter even in vacuum, getting these SEM pictures would be a considerable effort, especially under the current circumstances with limited personnel available due to the pandemic situation.

3) Impact of using different calibration methods. When showing the different VBS systems, I would like to see also a comparison to a VBS derived using a group contribution method or a fit to it (as e.g. in Stolzenburg et al., 2018 or Mohr et al., 2019). This would indicate which calibration method is more in line with this widely used approach, which does not rely on a direct volatility measurement.

Determining the VBS distributions with group contribution methods and comparing them to VBS distributions determined using direct volatility measurements is indeed an interesting topic, but we decided to leave that analysis out from our manuscript as we think it to be a whole topic of its own. One important issue is that most of the parameterisations were developed for measurements of gaseous compounds. When a thermal desorption step is included, the extend of thermal decomposition must be considered, i.e. that low-volatile but thermally labile compounds are detected as small fragments which will lead to a significant overestimation of their  $C^*$  values (see e.g. Buchholz et al 2020, Lopez-Hilfiker et al. 2015, Schobesberger et al. 2018, Stark et al. 2017).

However, we are currently working on this topic and will discuss it in more detail in future publications.

#### Minor:

1) P.1, l.31-32: I am missing a short discussion on other volatility measurement techniques, e.g. VTDMA setups. Please add this here.

Added reference to VTDMA.

2) P.2, l.39: I am missing some laboratory studies from the CLOUD team published recently, e.g. Wang et al. (2020, Env. Sci. Techn. & Nature), Stolzenburg et al. (2018, PNAS). Also missing is Mohr et al. (2019, Nat. Commun.). In all these studies the FIGAERO-CIMS was deployed quite successfully and they could be mentioned here for completeness.

Added Stolzenburg et al. 2018 and Mohr et al. 2019 to references listed at this line and additionally also added Wang et al. 2020 to the reference list of published calibration lines.

3) P.2, l.49: Also Wang et al. (2020, Env. Sci. Techn.).

Added Wang et al. 2020 to reference list, and updated Figure 1 and Figure S2 with their calibration line.

4) P.5, l.144: Did you constrain the width of the lognorm fit for the desorption? This could be necessary especially for unknown compounds, which might have isomers or fragments on the same mass yielding a bimodal structure.

The reviewer is right that often the fit needs to be constrained. As the calibration compound thermograms are “ideal”, lognormal fit can be applied to the whole thermogram, but in “real” data the fit usually needs to be constrained around the peak of the thermogram, especially if the thermogram is bimodal or broadened by the presence of isomers and/or fragments from thermal decomposition. Note that in the case of the presence of multiple compounds of different volatility, the  $T_{max}$  value may represent only the volatility of the dominant compound and ignores the contribution of the minor compounds with that sum formula. But it is also possible that the  $T_{max}$  value represents an “average” over multiple compounds, especially if the thermogram peaks of the isomers/fragments are too close to be distinguished. For such cases, the  $T_{max}$  method cannot capture all of the volatility information and a more sophisticated method is needed to separate the compounds (e.g. Positive Matrix factorisation, Buchholz et al. 2020)

5) P.6, l.185-187: If the inlet is initially at a different temperature, the supply of a constant heat rate will yield a different thermogram, as it takes longer to achieve the corresponding temperatures allowing more time for evaporation. Is this considered in then model? And how can we use calibrations performed at one temperature in comparison to measurements at different temperatures? Could the model resolve this?

The FIGAERO uses filters made of only PTFE. The filter holder and the moving tray are also machined from PTFE. One reason for that choice is the material's chemical inertness. But the main reason for choosing PTFE is its low thermal conductivity. Consequently, the temperature of the deposit is more directly controlled by the heat of the N<sub>2</sub> flowing through the filter, which is measured immediately upstream and hence well understood. The model therefore does not explicitly consider the heating of the filter material. But it does allow for "non-ideal" heating of certain parts of the deposit. The description of that non-ideality is fairly crude (details in Schobesberger et al., ACP, 2018). It has not been modelled as a function of heating rate, as that has not appeared necessary. The main "job" of the non-ideal heating in the model is to produce thermogram tails; it hardly affects  $T_{max}$ .

If the reviewer's latter two questions refer to the \*ambient\* temperature of the calibrations, the model is not currently set up to resolve resulting issues.

If the reviewer refers to extending the experimentally obtained "calibration curve" to  $T_{max}$  values beyond those provided by the observed  $T_{max}$  (illustrated e.g. in Fig. S2, and subject of Fig. S3), the model could in principle do that, but it would require asserting a relationship between saturation vapor pressures and vaporization enthalpies (e.g., see Fig. 7 in Schobesberger et al., 2018).

6) P.7, l.202: Repeat the atomizer solution concentration to put it into the context with the syringe concentrations. Also mention here the mode diameter of the particles used for calibration or even calculate the deposited mass for this type of calibration compared to the syringe method. This would put the two methods into comparison here.

Added more information to the section.

Line 208 onwards:

“For comparison, the starting concentration of the atomizer solution was 0.5 g L<sup>-1</sup> for each compound. The solution concentration gradually increased as the solvent evaporated from the solution. This led to a polydisperse, log-normal-shaped aerosol population with a mode diameter of 50 nm. From this distribution, particles equivalent to ~200 ng of aerosol mass were sampled onto the FIGAERO filter before desorption.”

7) P.8, l.231: Instead of mentioning the different scale, I would like to see a fourth panel in Fig 4 showing the filter in the same scale as in Fig. 5c! This would help to directly compare the different structures deposited on the filter.

Added fourth panel to Figure 5 (panel c) with 10 μm scale, taken as same sample as Fig. 5a). Original Fig. 5c) is now Fig 5d).

8) P.8, l.240: Also the larger diameters needed to explain the syringe calibration with model point into that direction. This is an important supportive argument and should be mentioned here.

We added the following to the revised manuscript:

Line 254 onwards:

Indeed, it was by building on these assumptions that the evaporation model succeeded in reproducing the observations in Fig. 4. With the much smaller surface area of the syringe deposited material, it requires more time to evaporate all the PEG-8 than from the equivalent amount of deposited aerosol particles. This time delay directly translates to a shift to higher observed  $T_{max}$  values. The desorption model mimics this change in surface-to-volume ratio by increasing the initial size of the modelled evaporating particle to 1.3 μm and 11 μm. But note that there are no individual spherical particles of that size on the filter.

9) P.8, l.251: Any hints why the different inlet behaves that way?

The positioning of the filter thermocouple affects the measured temperature of the desorption flow. It also affects the exact offset between the measured temperature and the temperature at the filter surface. To position the thermocouples in exactly the same position in two different inlets is quite difficult, so it is relatively hard to achieve exactly comparable measurements using separate inlets.

This is one of the reasons why a temperature calibration is necessary for each FIGAERO inlet and also every time the inlet is disassembled as disassembling the inlet may affect the position of the thermocouple.

10) P.8, 1.254: Why does it fail for PEG-8? Please elaborate on that.

In the model simulation, molecules that have desorbed from deposited particles are subsequently interacting with instrument surfaces, which are experiencing the same temperature ramp as the deposit, before being measured. That interaction is simulated by 100% initial absorption, and desorption as a function of  $C^*(T)$  and an optional instrument constant. (The latter is indeed the main tuning parameter for the model to reproduce observed  $T_{max}$  values). These interactions cause a delay. The delay translates to higher  $T_{max}$  and increases with decreasing  $C^*$  as well as decreasing particle size. Consequently, differences in  $T_{max}$  due to particle size disappear when  $C^*$  and particle size are sufficiently small, as  $T_{max}$  becomes controlled by those vapor-surface interactions. This is what we observe in the model outputs for PEG-8 (and somewhat also for PEG-7).

We believe that that is a shortcoming of the model, rather than of the experiments, because: (a) the thermograms were experimentally very well reproducible, and (b) the thermograms (in particular for PEG-8) were narrower for 80-nm particles than for 300-nm particles. From the model's point of view, observation (b) would suggest more ideal heating in the 80-nm case than in the 300-nm case, while the lower  $T_{max}$  would suggest less vapor-surface interactions. To affect that, 80-nm particles would need to be deposited somehow substantially differently on the filter than 300-nm particles. More likely instead, the model's current treatment of both non-ideality of heating and vapor-surface interactions (Schobesberger et al., 2018) are insufficiently close to reality in this case.

11) P.10, 1.295: Move "A more detailed description of the SOA production is shown in Ylisirniö et al., 2020." in front of the preceding sentence.

Sentence moved.

12) P.10, 1.299: 200 g mol<sup>-1</sup> seems quite low for alpha-pinene HOMs, e.g. Tröstl et al. used 300 amu as mean mass.

The reviewer is correct that 200 g mol<sup>-1</sup> is small compared to the mean molecular mass of alpha-pinene HOMs. However, when  $C^*$  is plotted in logarithmic space as in Fig.9, the change from 200 g mol<sup>-1</sup> to 300 g mol<sup>-1</sup> becomes negligible, as can be seen in the figure below. We therefore think that 200 g mol<sup>-1</sup> is adequate for our purposes.

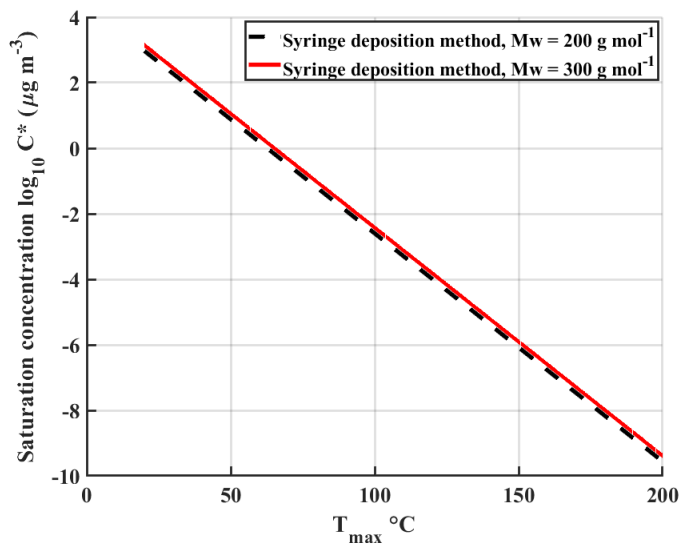


Figure 2. Figure 9 panel d) syringe deposition method theoretical line calculated with 200 g mol<sup>-1</sup> and 300 g mol<sup>-1</sup>.

13) P.11, l.355: Seems logical, but extremely difficult to realize in the lab. What would be the best alternative?

We are not completely sure what the reviewer means with this question as the sentence in the line 355 reads: “We note that these  $P_{sat}$  values have not been verified by other studies and are subject to corrections, but want to point out that harmonizing further FIGAERO calibrations by using PEGs would make future FIGAERO measurements more comparable to each other.”

We want to note that by word “harmonizing” we don’t mean a rigorous ISO-standard style calibration procedure, but simply that each FIGAERO would be calibrated with same compounds and using same  $P_{sat}$  values.

## Reviewer 2

### Major comment:

The manuscript deals with calibration issues, which means it deals with quantitative issues, and it compares to results from other references. Although the authors made aware of suited fitting procedures for data with errors in y and x (line 168f) there is no detailed error analysis nor are error bars shown in the Figures 1, 4, 7, 8, S2, S3. The only errors given are the statistical errors from averaging single measurements. I find that strange for a paper that deals with quantitative analysis and urgently suggest to add more detailed error analysis' and -discussion.

The reviewer is correct that more detailed description about the errors is needed. The main results of the paper are the  $T_{max}$  value measurements, i.e. the actual temperature measurements and its associated errors. The FIGAERO inlet uses two k-type thermocouples, which have typical measurement error of +/- 2.2 K. Additional ~1K of error is also introduced by the electronics of the measurement system. However, this total uncertainty of ~3 K can be thought of as a systematic error, rather than a random error. Therefore, the calibration procedure itself captures this uncertainty. Any random component of the temperature measurement error is then captured with repetitions and shown in standard deviations. An additional component to the error is introduced in the fitting of the asymmetric lognormal function over the measured thermograms. This error can be estimated by using the fitting routine's goodness-of-the-fit parameters, such as R-square value.

In Figures 1, and S2 the error bars are omitted for sake of clarity, but this is now pointed out in the captions and errors are discussed in the sect. 2.5.

Error bars and their description are now added to Figure 4 and explained in the caption.

In Figure 7, the error bars are omitted from the figures measured values as they are not distinguishable in the x-axis direction and do not add value to the plot. A range of the models results are however now shown in panel b) when using the uncertainties for evaporation enthalpy  $\Delta H$  shown in Krieger et al (2018). The y-axis error values are the same as in Figure 4. The range of the errors is now given in the figure caption:

“Error bars are omitted from the measured values in the figure for sake of clarity. In the panel b) whiskers show the range of model results when using uncertainties of evaporation enthalpy shown in (Krieger et al., (2018). The standard deviations of the for all measured points is panel a) is between 0.2-0.5 °C. In panel b) the standard deviations for measured points are between 0.2 – 1.3 °C.”

For Figure 8 error bars are now shown in the plot and the error analysis is explained in the supplement information S4. Briefly, the x-axis errors are calculated with propagation of error for both syringe injections and aerosol collections. The Y-axis errors are estimated by assuming Poisson-type counting statistics.

In Figure S3 the error bars are not shown as the idea of the figure is to be mainly speculative on how the  $P_{sat}$  values of higher order PEG-compounds could possibly be estimated.

Minor comments:

line 44: References should be given already here, in addition to the link to section 2.5.

Moved citations.

line 82: Are these heating rates really so accurate (2 decimal digits)? The experiments do not lead to the same maximum temperature, does that effect the integrals under the thermograms?

We decreased the accuracy of the ramp rate to one digit. For the integration, the thermogram is integrated against time and not temperature, as data is measured in counts per second. Therefore, maximum attained temperature does not affect the integral value as long as it was high enough for all material to desorb from the filter.

line 97: From PEG-4 to PEG-8. In integer steps? Please, specify precisely which PEG's you used.

Text has been modified to mention all used PEG-compounds.

Line 99:

The used PEG standards were PEG-4, PEG-5, PEG-6, PEG-7 and to PEG-8.

line 115-120: Did you use a neutralizer ? If yes, which? How did you handle multicharged particles in the selection by DMA. This needs to be explained, and potential errors need to be estimated and discussed.

The TSI model 3082 SMPS-platform contains a Kr-85 radioactive neutralizer and the measurement software automatically corrects for multicharged particles. When used in DMA mode for monodisperse aerosols, the particle size was selected from the falling edge of the polydisperse particle distribution, keeping the amount of multicharged particles at a minimum. For example, the measured mode diameter of the polydisperse aerosol distribution was ~50nm and we selected 100 nm monodisperse particles for the sensitivity measurements.

Figure 6: I don't see a real difference between with and w/o particles. What made you think that the marked white blobs are particles? The marking with the red circles is too suggestive. I propose to leave them out. In this context: In the ambient with aqueous particles and RH, wouldn't the particles flow together and merge anyhow? I would still believe that even considering that, particle deposition should lead to finer structures compared to evaporating droplets deposited by syringe. What could be the influence of a fast evaporating solvent the structure of the dried deposit? Did you do experiments with others solvents?

The reviewer is right that it is indeed difficult to distinguish the PEG-8 particles from the filter material. We base our estimation on the quantity of the white "blobs" seen in the picture with deposited particles compared to the clean filter.

When considering aqueous particles, the distance between the collecting filter fibres compared to the size of the collected aerosol particles is large enough that the particles should not meet each other unless using very high mass loading when collecting the sample. The aerosol particles are also so small that intermolecular forces between the particles and filter fibres should be strong enough to prevent them from moving around in the filter by the collection flow drag. Note that for high sample mass on filters, sample mass dependent shifts of  $T_{max}$  have been observed (Huang et al. 2018, Atmos. Chem. Physics) which may be connected to particles interacting on the filter.

As the PEG-8 molecules are floating freely in the acetonitrile (ACN) solution without diffusion limitations, the evaporation rate of the solvent should not affect how the PEG-8 molecules deposit onto the filter.

As for other solvents, to dissolve PEGs a polar solvent is needed. However, we observed oligomerisation reaction for PEG4 when using alcoholic solvent (methanol). In addition to ACN we did test ethyl acetate and deionized water as solvents for both the syringe and the atomizer method but did not take SEM pictures with these solutions. We decided to use ACN instead of Ethyl Acetate as its less volatile. The higher volatility of ethyl acetate could have caused problems in atomization as the atomizer solution concentration would have changed too rapidly as the solvent evaporates. Additionally, the PTFE-filter is less phobic towards ACN than it is towards water, which eases the syringe deposition experiments. For these reasons, we recommend using ACN as solvent for PEGs. However, if ACN is not available, it is possible to replace ACN with another aprotic/non-alcoholic, somewhat polar solvent at least in the atomizer method.

line 216 and Line 219: “We were largely able to reproduce our measurement results: :” and “with practically no free parameters”, what do ‘largely’ and ‘practically no’ mean in this context, please, rephrase or specify.

We specified and tried to clarify those two sentences, now reading as follows:

Line 228 onwards:

“We were able to reproduce our measured  $T_{max}$  values within 10 °C using the evaporation model to simulate the evaporation of mixed PEG 4-8 particles (for simplicity assuming equal mole fractions for all PEG). For PEG-5 and -6, Figure 4 shows excellent agreement between measured and modelled  $T_{max}$  values for the atomizer method (within a couple of °C), deteriorating to a difference of about 10 °C for PEG-8. This broad agreement here is remarkable in so far, as in this case the model was run with no vapor-surface interactions, i.e. no tuning in regards to resulting  $T_{max}$ , which are therefore a direct result of the input values for  $C^*$  and  $\Delta H$ .”

line 326-329: This statement should be appear in the result section before.

Moved the paragraph to Section 3.1.

Typos:

line 30: the these, cancel “the”

Done.

line 52: "stems", turn to plural

Done.

line 62: Bannan et al. 2019, add the bracket to year

Done.

line 70: "that atomizer method", add "the"

Done.

line 486(Figure 1): "for the further divergence", didn't you mean "larger divergence?"

Replaced with "large":

"...for the large divergence..."

line S48: "d", should be "f"

Done.

## Reviewer 3:

### GENERAL

Modeling (Page 6, 3rd paragraph; page 7 last lines; page 8, 3rd and last paragraphs, page 11 1st paragraph): The model brings enough insight to justify itself for the paper, but I think it could be better tied to the results. As the model predicts the effect of particle diameter, maybe this aspect could be dealt with first. One could estimate the surface to volume ratio of the residue to that of the fitted 11  $\mu\text{m}$  diameter particles. It seems that an order of magnitude agreement would be achieved with a reasonable residue thickness estimate. Another thing: why is the model insensitive to particle diameter for PEG-8? The authors might like to check for papers that have come out after preparing the manuscript.

We believe that the storyline works well enough as it is, and it is more in line with how our understanding progressed during this study. We first had the observation of increased desorption temperatures for syringe methods, and blaming that on reduced S:V was one of several initial hypotheses, but the one that crystallized as the most plausible explanation. Our evaporation model is able to simulate that effect, in its simplifying approach, but nonetheless able to roughly quantify it, so we agree that the obtained numbers are providing useful “ballparks”. (The SEM pictures were then taken last.)

Estimating the S:V of the residue, based on the SEM pictures, is an interesting approach – if very qualitative only, as the “reasonable residue thickness estimate” is a major uncertainty. But if we anyway, for example, looking at Fig. 5, maybe a good guess would be a residue consisting of  $20 \times 20 \mu\text{m}^2$  blocks with a depth of  $1 \mu\text{m}$ ? The corresponding S:V is  $2.2 \mu\text{m}^{-1}$ , equivalent to the S:V of a sphere (particle) of diameter  $2.7 \mu\text{m}$ . Indeed, a reasonable order of magnitude agreement is achieved (the model using  $1.3 \mu\text{m}$ ; Fig. 4). But a major problem remains with the lack of depth information obtainable from the SEM images, as up to the filter thickness ( $\sim 150 \mu\text{m}$ ), a suitable residue thickness can mostly be found (“estimated”) to come up with the particle size value desired. Indeed, one could argue that, vice versa, SEM images plus modelled particle size could be used to estimate residue thickness. Adding to that argument are the similarities regarding apparent residues between Fig. 1 panels a) and b) in this document above, despite different solution concentrations used (0.01 and 0.25 g/L, respectively), whereas the model would use particle sizes of 1.3 and  $>11 \mu\text{m}$ , respectively (Fig. 4). But if we keep with  $20 \times 20 \mu\text{m}^2$  patches, we only need to increase their depth, for example to  $5 \mu\text{m}$ , and the corresponding particle size would increase to  $10 \mu\text{m}$ . Voilà. So those calculations are able to provide reasonable numbers. That is encouraging, but we feel that they remain poorly constrained by our observations (plus model simulations), and we do not learn much more, and only with high uncertainties.

Regarding PEG-8/Fig. 7, please see response to Reviewer 1, comment 10.

Regarding the new papers that have been published during the review progress, we have added Wang et. al., (2020) calibration line to Figure 1 and Figure S2.

## SPECIFIC COMMENTS

Abstract:

There would be room for specific numbers on the effects of the methods on peak temperature, pressure and concentration.

Added an example about the difference in  $T_{max}$  between atomizer method and syringe method and how big effect this would cause in  $C^*$  space.

Line 22:

“For example, we found a difference of  $\sim 15$  °C in observed  $T_{max}$  values between the atomizer method and the syringe method when using the lowest solution concentration (0.003 g L<sup>-1</sup>). This difference translates to up to 3 orders of magnitude difference in saturation concentration  $C^*$  space.”

Methods:

Page 4 and onwards: I understand the concentration probably affects the residual ring pattern, but it would be nice to also show the deposited solute mass.

Deposited solute masses are already being reported in the end of the Sect. 2.3. “The mass deposited varied between 9 ng and 500 ng, depending on the used concentration.” In the SEM pictures amount of deposited mass was 30ng. This information is now added to the figure caption.

Eq (3) and related texts:  $C^*$ -space is referred to later in the text several times, as is customary to the field. On the other hand, this paper (or the supplement) does not provide the physical properties of the compounds needed to convert the saturation pressure values to concentrations. Including the equation is therefore of limited value. Maybe the properties could be listed in the supplement? Or then just point out here that this is a linear function. BTW: molecular weight/mass should be changed to molar here, and later when appropriate.

If the reviewer refers to  $P_{sat,meas}$  or  $M_w$  as physical properties of the compounds, the  $P_{sat,meas}$  value is determined from measured  $T_{max}$  value using eq(2) and  $M_w$  is determined directly from the CIMS data. This is now clarified in the text and molecular weight is changed to molar mass.

Line 164:

“where  $M_w$  is the molar mass of the compound (in units of g mol<sup>-1</sup>) determined with the CIMS,”

## Results and discussion

Figure 3 and related texts: Overall this is a nice set, conveying the message. I have some minor points: -Please harmonize the two panes for marker and text sizes -There would be more room to spell out the Saturation vapor pressure within the caption than on the axis. This is shortened to Saturation pressure elsewhere in the text. -I guess the lines are just to guide the eye. Why are they missing from the b) and why is the PEG atomizer data included? -I propose checking (dashed) horizontal lines to the  $P_{sat}$  values -Please refer to supplement here for the  $P_{sat}$  values -I did not find mention of the sources of the carboxylic acid  $P_{sat}$  values. These should be added.

Figure 3 is now modified as requested. Used  $P_{sat}$  values for carboxylic acids and their reference are listed in Table S1 and this is mentioned in the text.

The lines connecting the dots in Fig. 3a) are indeed to guide the eye. They are however missing from Fig 3b) from carboxylic acids as the data is more compacted and thus would make the figure harder to read. Also, the PEGs are a homologous series, whereas the acids are not. The PEG atomizer data is included for easier comparison between the two panels as the x-axis is different in each panel.

Figure 5: The scale bar text is too small. Although is implicitly clear, maybe the caption should spell out that this is after solvent evaporation. Maybe use the word residue?

Increased the scale bar text and added fourth panel as suggested by Reviewer 1. New panel shows zoomed in picture of panel a). Changed the word 'PEG-8 "ring"' to 'PEG-8 residue'.

Figure 6: I know there is little that can be done here, but it is practically impossible to tell the particles apart from the filter. The marked particles are approximately one micrometer in diameter, not 300 nm. Any explanation?

It is indeed hard to distinguish the collected particles from the filter material. We base our estimation on the quantity of the white "blobs" seen in the picture with deposited particles compared to the clean filter. The amount of material collected onto the filter was substantially higher than what would be normally collected during experiments, to ensure the identification of the particles from the filter material. It is possible that some of particles have coagulated in the filter and formed bigger particles.

Page 8, last paragraph and figure 7: Explain what the difference in the inlet was, and why it affects the  $T_{max}$  values.

The other inlet used in this paper was a slightly modified version from the general Aerodyne inlet. The two inlets differ geometrically slightly from each other in terms of pin hole and thermocouple positioning. However, as the point of the calibration is to ensure that different FIGAERO systems are comparable to each other, slight changes in the inlet geometry are not crucial. The largest source of error regarding  $T_{max}$  values comes from the exact positioning of the filter thermocouple, which is individual to each FIGAERO inlet, and is an important reason to use harmonised calibration method between different FIGAERO instruments.

Figure 8: Nice result, but as this is calibration, should there not be an error estimate?

Error bars are now added to the figure and the error analysis is explained in the supplement information.

Page 10, 2nd paragraph: “Note that the heating ramp rates in these calibrations were done with faster heating ramp rate...” This sentence can be shortened quite a bit. Apart from that, maybe the authors would like to discuss the effect of the ramp rate in the light of this paper...

We modified the sentence:

Line 317:

“Note that the calibrations shown in this paper used faster heating ramp rates than what was used in the SOA measurements, introducing an overall small systematic error (<1 order of magnitude in  $C^*$  space) towards higher saturation concentrations.”

The effect of the used ramp rate on the observed  $T_{max}$  values is discussed in Sect. 3.3, last paragraph, and the effect is shown in Figure 7.

# On the calibration of FIGAERO-ToF-CIMS: importance and impact of calibrant delivery for the particle phase calibration

Arttu Ylisirniö<sup>1</sup>, Luis [M. F. Barreira](#)<sup>1,2</sup>, Iida Pullinen<sup>1</sup>, Angela Buchholz<sup>1</sup>, John Jayne<sup>3</sup>, Jordan E. Krechmer<sup>3</sup>, Douglas R. Worsnop<sup>3</sup>, Annele Virtanen<sup>1</sup>, and Siegfried Schobesberger<sup>1</sup>

<sup>1</sup>Department of Applied Physics, University of Eastern Finland, FI-70211 Kuopio, Finland.

<sup>2</sup>Atmospheric Composition Research, Finnish Meteorological Institute, Helsinki, Finland.

<sup>3</sup>Center for Aerosol and Cloud Chemistry, Aerodyne Research, Inc., Billerica, MA, USA.

*Correspondence to:* Arttu Ylisirniö (arttu.ylisirnio@uef.fi)

## Abstract

The Filter Inlet for Gases and AEROsols (FIGAERO) coupled with a Time-of-Flight Chemical Ionization Mass Spectrometer (ToF-CIMS) enables online measurements of both gas-phase and particle phase chemical constituents of ambient aerosols. When properly calibrated, the incorporated particle filter collection and subsequent thermal desorption enable the direct measurement of volatility of said constituents. Previously published volatility calibration results however differ from each other significantly. In this study we investigate the reason for this discrepancy. We found a major source of error in the widely used syringe deposition calibration method that can lead to an overestimation of saturation vapour pressures by several orders of magnitude. We propose a new method for volatility calibration by using atomized calibration compounds that more accurately captures the evaporation of chemical constituents from ambient aerosol particles. For example, we found difference of  $\sim 15^\circ\text{C}$  in observed  $T_{max}$  values between the atomizer method and syringe method using lowest solution concentration ( $0.003\text{ g L}^{-1}$ ). This difference translates up to 3 orders of magnitude difference in saturation concentration  $C^*$  space. We justify our claim with evaporation modelling and direct Scanning Electron Microscopy imaging, while also presenting possible error sources of the atomizer method. We finally present how typical calibration parameters derived with both methods impact the Volatility Basis Set (VBS) derived from measurements of Secondary Organic Aerosols (SOA).

## 1 Introduction

Organic aerosol (OA) has received substantial attention during the past decades due to its large fraction of the total atmospheric aerosol mass around the globe (Hallquist et al., 2009; Jimenez et al., 2009). The tendency of the organic matter to stay in the particles or evaporate is dictated by the volatility of the OA constituents. This information is also critical for atmospheric models for accurate treatment of secondary organic aerosols (SOA) in ~~the~~ these models (Sporre et al., 2020). During the past

years, several techniques have been developed to measure the physicochemical properties of the OA, including volatility. A major class of these techniques relies on heating the aerosol particles followed by compositional analysis of the evaporating molecules by mass spectrometers. Examples of these techniques are the [Volatility Tandem Differential Mobility Analyzer \(VTDMA, Hong et al., 2017\)](#), Thermal-Desorption Chemical Ionization Mass Spectrometer (TD-CIMS, Smith et al., 2004), the Micro-Orifice Volatilization Impactor Coupled to a Chemical Ionization Mass Spectrometer (MOVI-CIMS, Yatavelli and Thornton, 2010) and the Chemical Analysis of Aerosols Online – Proton Transfer Reaction Mass Spectrometer (CHARON – PTR-MS, Eichler et al., 2015). Another technique, which has gained popularity, is the Filter Inlet for Gases and AEROsols (FIGAERO) coupled with Time-of-Flight Chemical Ionization Mass Spectrometer (ToF-CIMS). Originally introduced by Lopez-Hilfiker et al., (2014), this technique has been employed in numerous field and laboratory studies (e.g. D’Ambro et al., 2017; Breton et al., 2018; Isaacman-Vanwertz et al., 2018; Riva et al., 2019; Mohr et al., 2019; Stolzenburg et al., 2018). The FIGAERO inlet enables semi-continuous gas-phase and particle-phase measurements of aerosol. The latter is done via filter collection followed by heating of the collected aerosol particles and simultaneous sampling of desorbing compounds, which can be identified and quantified by the ToF-CIMS. It also enables extraction of volatility information of the particle phase through the investigation of thermograms: the measured signal as a function of linearly ramped desorption temperature. In particular, the temperature of peak signal ( $T_{max}$ ) has turned out to be a useful measure (see Sect. 2.5 for details, [\(Lopez-Hilfiker et al., 2014; Stark et al., 2017; Bannan et al., 2019; Joo et al., 2019; Nah et al., 2019; Ye et al., 2019; Wang et al., 2020\)](#)). When accurately calibrated, these measured  $T_{max}$  values can be directly related to saturation vapor pressure values ( $P_{sat}$ ) and used to estimate the volatility of the chemical constituents in the aerosol particles (Lopez-Hilfiker et al., 2014). However, only a considerably small amount of studies has taken advantage of this possibility and have reported the calibration procedures used for quantifying the relationship between  $T_{max}$  and  $P_{sat}$  [\(Lopez-Hilfiker et al., 2014; Stark et al., 2017; Bannan et al., 2019; Joo et al., 2019; Nah et al., 2019; Ye et al., 2019\)](#). Fig. 1 reproduces the published calibration results known to us, for a direct comparison. It illustrates remarkable discrepancies between individual calibration results. One issue here is that  $P_{sat}$  values used in the calibration fits, either literature-based or model-derived, vary significantly between studies (by up to 4 orders of magnitude for the same compound, see Table S1). These discrepancies stem in part from notorious difficulties in measuring and estimating the saturation vapor pressure of low-volatility compounds. Bannan et al., (2019) proposed a solution to this problem by using series of polyethylene glycol (PEG) compounds, which showed good agreement of measured  $P_{sat}$  values between different experimental methods (Krieger et al., 2018). Other issues may arise from differences in the exact calibration methods. All calibration lines shown in Figure 1 have been produced by depositing known amounts of calibration compounds in solution on the FIGAERO filter using a micro syringe (later referred as syringe method). However, there is a remarkable wide variation in the level of detail at which published calibrations have been described; specifically, in terms of used solvent, solution concentrations and amount of material deposited onto the filter.

In this study we investigated the possible reasons for the large discrepancies between many reported calibration lines (Fig. 1). We repeated the calibration measurements described in Bannan et al., (2019) with PEG (4-8) compounds, and a set of

carboxylic acids, and probed the effect of different solution concentrations on the calibration results. As the FIGAERO inlet itself is initially designed to study aerosol particles, we further conducted calibration experiments via atomizing the calibration compounds (later referred as atomizer method) and found remarkable differences compared to the experiments performed via micro syringe depositions. Furthermore, as several studies performed with FIGAERO-ToF-CIMS use the syringe method also to calibrate for the sensitivity of the instrument (Liu et al., 2016; Breton et al., 2019), we compared the two previously mentioned methods also in terms of sensitivity calibrations. We furthermore investigated potential impacts of different heating ramp rates and aerosol particle sizes to results using the atomizer method. In light of our results, with further support from evaporation modeling and direct scanning electron microscopic (SEM) measurements, we propose that the atomizer method should from now on be used for calibrating the FIGAERO-ToF-CIMS volatility range.

## 2 Methods

### 2.1 FIGAERO-ToF-CIMS

The operation of the FIGAERO inlet is thoroughly explained in previous publications, with the original inlet design described in Lopez-Hilfiker et al., (2014) and a commercialized design by Aerodyne Research, Inc. described in Bannan et al., (2019). In short, the FIGAERO inlet enables measurements for both particle-phase and gas-phase constituents by the use of two separate pin holes leading into the mass spectrometer. While the gas phase is sampled through one pin hole, the other is kept closed and aerosol particles are simultaneously sampled onto a PTFE filter (Zefluor, Pall Corp. 2  $\mu\text{m}$  pore size). After sufficient particle mass has been collected onto the filter, the filter is moved in front of the second pin hole and the gas phase pin hole is blocked. Chemical constituents are then evaporated from the filter into the mass analyser by a nitrogen flow that is gradually heated, ramping at a constant rate from room temperature to 200 °C, as measured just above the filter. The rate of the heating ramp is adjustable, and for this study, we used heating rates of 11.4 and 6.325 K min<sup>-1</sup> corresponding to ramping times of 15 and 30 minutes. In this study we used the commercial version produced by Aerodyne Research Inc. for the solution concentration and heating ramp rate experiments and a custom design with small deviations from the commercial version (different nitrogen flow heating system and smaller distance between the two pinholes) for the sensitivity and particle size experiments.

The ToF-CIMS (Tofwerk AG, Aerodyne Research, Inc.) was operated with an iodide-ionization scheme (Iyer et al., 2017; Lee et al., 2014) and at a mass resolution of 4000-5000. Iodide ions were generated by passing an ultrapure nitrogen flow of 1 SLPM over a permeation tube containing methyl iodide (CH<sub>3</sub>I) and through a commercial Po-210 source (Model P-2021, NRD Static Control LLC) into the Ion Molecule Reaction chamber (IMR) of the instrument. The IMR was operated at a pressure of 100 mbar which was actively controlled.

## 2.2 Sample preparation

In this study, polyethylene glycols (PEG, Polypure AS) and carboxylic acids were used as standards to test the effect of solution concentration on the results. Acetonitrile (ACN, Fisher Scientific 99.8% purity) was chosen as a solvent for stock solutions since it does not react with any of the compounds used in the study whereas for example methanol, the most commonly used solvent, was found to polymerize PEGs into higher order polymers. The used PEG standards were ~~from~~ PEG-4, PEG-5, PEG-6, PEG-7 and ~~to~~ PEG-8. The used organic acids were pimelic acid (Sigma Aldrich, 98% purity), azelaic acid (Sigma Aldrich, 98% purity), sebacic acid (Sigma Aldrich, 99% purity), palmitic acid (Sigma Aldrich, 99% purity), oleic acid (Sigma Aldrich, 99% purity) and stearic acid (Sigma Aldrich, 95% purity). Both stock standard solutions of individual components and mixtures of studied analytes were prepared and tested.

## 2.3 Syringe deposition method

In the syringe deposition method, a known amount of the prepared standard solutions was deposited onto the FIGAERO filter via a microliter syringe (10  $\mu$ l, Hamilton Co.). To access the filter, the filter holder tray was pushed out from the body of the inlet until the filter was exposed. The amount of deposited calibration standards was calculated from the solution concentration and volume of deposited solution. After deposition, the solvent is assumed to quickly evaporate from the filter, leaving behind the less volatile calibrant analyte. An illustration of the method is shown in Fig. S1 a). Solution concentrations for the syringe deposition method were 0.1, 0.01 and 0.003 g L<sup>-1</sup> for the PEGs and 0.5, 0.1 and 0.01 g L<sup>-1</sup> for the acids. The deposited volume of standard solution was 1  $\mu$ l, which provided a sufficient calibrant mass on the filter to ensure a clear signal. The mass deposited varied between 9 ng and 500 ng, depending on the used concentration. For sensitivity calibrations, PEG-7 standard solutions (0.01 g L<sup>-1</sup>) were used. The deposited volume was 1-5  $\mu$ l, which corresponded to a deposited mass of 10-50 ng.

## 2.4 Atomization method

In atomization method, PEG standards were prepared in an initial concentration of  $\sim$ 0.5 g L<sup>-1</sup> each in a mixture in acetonitrile (see Sect. 2.2). For delivering the calibrants to the filter, the solution was then atomized with a commercial atomizer (TSI Aerosol generator model 3076). Atomized particles were passed through a dilution volume and were continuously monitored with a Scanning Mobility Particle Sizer (SMPS, TSI model 3082 platform coupled with a TSI model 3775 Condensation Particle Counter, CPC). The dilution volume ensured that all solvent had completely evaporated from the particles before size measurement/classification and filter collection. We studied both polydisperse (mode diameter  $\sim$ 60nm) and monodisperse aerosol particles. Monodisperse particles were size selected from the polydisperse aerosol population with a Differential Mobility Analyzer (DMA). Schematics of the respective calibrant delivery setups are shown in Figure S1 panels b) and c).

Before the actual filter collection, the particles were passed through the aerosol collection port of the FIGAERO-inlet to maintain constant flow conditions in the setup while the collecting filter was in the desorption position and flushed with room

air temperature nitrogen. When the particle concentration had stabilized, the filter was moved into the aerosol flow and the collection started. The amount of collected material was calculated based on particle size (determined by SMPS, assuming that all particles were spherical), CPC particle counts, collection time, and flow rate through the filter.

As the solvent used in the atomization method actively flushed the walls of the atomizer, dissolving any dissolvable material from to walls to the solution, it was essential to thoroughly clean the atomizer before measurements. The atomizer was also periodically used with pure solvent and the output was monitored with SMPS to ensure that all measured particles consisted purely of calibration compounds.

During the atomization progress, the initial solution concentration slowly increases as part of the solvent evaporates inside the atomizer. However, this change of concentration only impacts the size distribution of the formed aerosol particles, which was continuously monitored. In the atomizer method measurements, collected mass loading on the filter ranged from 100 to 200 ng. Typical collection times ranged from 10 s (polydisperse sample) to few minutes (monodisperse sample). For sensitivity calibrations performed with PEG-7, 100 nm particles with a similar mass loading range were used with initial atomizer solution concentration of 0.5 g L<sup>-1</sup>. The measurement setup shown in Fig. S1 c).

## 2.5 Data analysis, $T_{max}$ determination and calibration line fitting

All ToF-CIMS data was pre-processed with Tofware (version 2.5.11 including FIGAERO plugin, Aerodyne Research, Inc.) running in the Wavemetrics Igor 7 programming environment and further postprocessed with custom MATLAB scripts (The MathWorks, Inc.).

For obtaining  $T_{max}$  values from the thermograms, the data was first smoothed by fitting an asymmetrical lognormal function across the peak of each thermogram. The assigned  $T_{max}$  values corresponded to the maxima of these functions (Figure 2 panel a)).

Obtained  $T_{max}$  values were fitted against natural logarithm of  $P_{sat}$  literature values, which leads to a near-linear relationship

$$\ln(P_{sat,lit}) = aT_{max} + b, \quad (1)$$

where  $a$  and  $b$  are fitted parameters. Saturation vapor pressure values for any measured compound ( $P_{sat,meas}$ ) can then be estimated by

$$P_{sat,meas} = \exp^{aT_{max,meas} + b}, \quad (2)$$

160 where  $T_{max,meas}$  is the measured  $T_{max}$  of the compound. In the field of organic aerosol studies, it is customary to express volatility  
in terms of saturation concentration ( $C^*$ ). ~~Estimated -Saturation-saturation~~ vapor pressures can be converted to saturation  
concentration following the ideal gas law:

$$C^*(\mu\text{g m}^{-3}) = \frac{P_{sat,meas}M_w}{RT} 10^6, \quad (3)$$

165

where  $M_w$  is the ~~molecular-molar weight-mass~~ of the compound (in units of  $\text{g mol}^{-1}$ ) ~~determined with the CIMS~~,  $R$  is the  
universal gas constant ( $8.314 \text{ J mol}^{-1} \text{ K}^{-1}$ ) and  $T$  is the temperature for which the original  $P_{sat,lit}$  values were determined (in  
units of K; typically, as in our case, for 298 K).

170 As both  $P_{sat,lit}$  and  $T_{max,meas}$  can have significant uncertainties, an appropriate fitting method should be chosen that accounts for  
errors in both variables ~~and appropriate fitting uncertainties should be shown with the fitting results~~. In this study, we used the  
bivariate least squares method (York et al., 2004) ~~in Fig. 2 b~~, which was implemented in MATLAB as shown in Pitkänen et  
al., (2016). When uncertainties were not available, as was the case with lines in Fig. 1 ~~and Fig. S2~~, Deming regression was  
used. ~~In these cases, fitting uncertainties are not shown for sake of clarity~~. For a thorough discussion of linear fitting methods  
175 while taking into account measurement uncertainties in both variables, see Mikkonen et al., (2019).

## 2.6 Evaporation model description

In this study, we also compare experimental results with the simulation results of a model that was designed to interpret  
FIGAERO-ToF-CIMS observations. The model is described in detail in Schobesberger et al., 2018. It simulates the molecule-  
wise evaporation of aerosol particles from the FIGAERO filter in a clean nitrogen flow, using a modified form of the Hertz-  
180 Knudsen equation. Accordingly, peak-shaped thermograms arise from the linearly ramped sample heating due to the fast  
increase of  $P_{sat}$  (and  $C^*$ ) with temperature (Clausius-Clayperon relation). The model demonstrated how  $T_{max}$  depends near-  
linearly on  $\log(P_{sat})$  as the enthalpy of vaporization generally increases with decreasing  $P_{sat}$ , in agreement with observations  
(cf. Fig. 1). The model also allows for including interactions between desorbed vapours and instrument surfaces, which can  
lead to an increase in  $T_{max}$ , as well as non-ideal heating, which broadens simulated thermograms and adds tailing, hence  
185 potentially better reproducing observed thermogram shapes.

## 2.7 Scanning Electron Microscope pictures

To gain information about the difference between atomizer collection and syringe deposition, we took Scanning Electron  
Microscope (SEM) pictures of the FIGAERO filters with PEG deposited onto the filter with either method. The employed  
instrument consisted of a Sigma HD Variable Pressure Field Emission Gun – SEM (VP FEG-SEM, Carl Zeiss NTS,  
190 Cambridge, UK) with a Variable Pressure Secondary Electron (VPSE) detector using an acceleration voltage of 15 kV. The

pictures were taken in a 20 Pa nitrogen atmosphere. As SEM pictures are taken in very low pressures, we deposited only PEG-8 to the filter as it had the lowest vapor pressure of the used PEGs and was thus least likely to evaporate in the vacuum during the imaging.

195 For preparing the FIGAERO filters for the SEM when using the syringe method, we attached the filters to a horizontal sample holder using double sided carbon tape and deposited the volume in the middle of the filter in same fashion as in normal syringe method measurement, before moving the holder into the SEM vacuum chamber. For investigating deposition using the atomizer method, we collected 300 nm monodisperse particles into the filter for 20 minutes after which the filter was attached to an identical sample holder and moved into the SEM within 15 minutes after the collection.

## 200 **3 Results and discussions**

### **3.1 Solution concentration effect**

We examined a range of solution concentrations for the syringe deposition method, with both PEGs and carboxylic acids. PEGs were measured as individual solutions and as a mixture. Carboxylic acids were measured as a mixture. With PEGs, we did not observe significant difference in  $T_{max}$  values between mixture and individual solutions. Figure 3 shows a shift of measured  $T_{max}$  to higher temperatures with increasing solution concentration, both for PEG compounds (Fig. 3a) and for carboxylic acids (Fig. 3b). The shown  $T_{max}$  values are averages of three repetitions. Exact  $T_{max}$  values with standard deviations are shown in Table S2 and Table S3.  $P_{sat}$  values of carboxylic acids are shown in Table S1. Figure 3a also includes reported  $T_{max}$  values from Bannan et al., (2019) as a reference, as they used PEG compounds with solution concentrations of  $\sim 2 \text{ g L}^{-1}$ . Both panels also show the  $T_{max}$  values we measured with the atomizer method, which yield the lowest  $T_{max}$  values with both sets of compounds. For comparison, the used starting concentration of atomizer solution was  $0.5 \text{ g L}^{-1}$  per compound, which gradually increased as the solvent evaporated from the solution. This led to polydisperse log normal aerosol population with mode diameter of 50 nm. From this  $\sim 200 \text{ ng}$  of aerosol mass was sampled into the FIGAERO filter before desorption.

The results shown in Figure 3 clearly show a dependence of measured  $T_{max}$  value on solution concentration deposited by syringe, with higher concentrations leading to higher  $T_{max}$ , whereas lowest  $T_{max}$  values are measured when using the atomizer. Even though  $T_{max}$  values from the lowest solution concentration of  $0.003 \text{ g L}^{-1}$  in PEG measurements approach the atomizer results, there is still a difference of  $\sim 15 \text{ }^\circ\text{C}$  between the results. This difference would manifest in 1-2 orders of magnitude in difference in estimated saturation pressure. Note that PEG-4 was not visible in the mass spectrometer data for the atomizer and the lowest solution concentration measurements. We suspect that its evaporation from the filter and from the particles is so rapid in these cases, that it has already evaporated before the start of the measurements, or, in other words, that its hypothetical  $T_{max}$  lies below or too close to room temperature. This is in line with the relatively high vapor pressure of PEG-

4. Its  $\log_{10}(C^*)$  value of 3.12 groups it into the class of Intermediate Volatile Organic Compounds (IVOC), as described by Donahue et al., (2012), which have been shown to readily evaporate from particles (Li et al., 2019; Yli-Juuti et al., 2017).

225 In Fig. S2 we show again previously reported calibration lines shown in Fig. 1, now updated with calibration lines acquired in this study with both the atomizer (solid green line) and the syringe method (conc. 0.1 g L<sup>-1</sup>, solid blue line). The area between the two solid lines encompasses almost all other reported calibration lines. It should be noted that even though the calibration lines extend all the way to 200 °C,  $T_{max}$  values used for the fitting are below 120 °C in almost all the studies.

230 We were able to reproduce our measured  $T_{max}$  values within 10 °C using the evaporation model to simulate the evaporation of mixed PEG 4-8 particles (for simplicity assuming equal mole fractions for all PEG). For PEG-5 and -6, Figure 4 shows excellent agreement between measured and modelled  $T_{max}$  values for the atomizer method (within a couple of °C), deteriorating to a difference of about 10 °C for PEG-8. This broad agreement here is remarkable in so far, as in this case the model was run with no vapor-surface interactions, i.e. no tuning in regards to resulting  $T_{max}$ , which are therefore a direct  
235 result of the input values for  $C^*$  and  $\Delta H$ . ~~We were largely able to reproduce our measurement results using the evaporation model to simulate the evaporation of mixed PEG 4-8 particles (for simplicity assuming equal mole fractions for all PEG). Figure 4 shows decent agreement between measured and modelled  $T_{max}$  values for the atomizer method, considering that the model was run with practically no free parameters in this case.~~ With increasing initial size of the modelled evaporating particle, the modelled  $T_{max}$  shift to higher values, due to the decreasing surface-to-volume ratio. By simply adjusting that size ( $D_p$ ), to  
240 1.3  $\mu\text{m}$  and 11  $\mu\text{m}$  diameter particles, respectively, the model indeed reproduced remarkably well the  $T_{max}$  values obtained with the syringe method for 0.01 g L<sup>-1</sup> and 0.1 g L<sup>-1</sup>.

### 3.2. Scanning Electron Microscope picture

245 Figure 5 panel c) shows magnification of the filter shown in panel a) and panel d) shows a magnification of the filter at the edge of the “PEG-8 ring” shown in panel b), showing how the PEG forms a layer on top and possibly also inside the filter. We emphasize that as SEM cannot distinguish deposited material situated inside the filter, the shown images should be considered as a qualitative evidence.

Figure 6 shows magnified SEM pictures of a FIGAERO filter (note different scale compared to Fig. 5). Panel a) shows a clean  
250 FIGAERO filter without collected particles, and panel b) shows a filter with collected 300 nm particles.

Even though qualitative at nature. Fig. 5 and Fig. 6 clearly demonstrate how differently the calibration material deposits onto the FIGAERO filter, depending on which method is used. We hypothesize that a vast difference in the surface-to-volume ratio of the deposited material, as implied by the SEM pictures, is particularly crucial in explaining the differing  $T_{max}$  results. We  
255 expect the molecular desorption rate of the deposit in clean nitrogen to be proportional to its total exposed surface area (Hertz-

Knudsen equation; Cappa et al., 2007; Schobesberger et al., 2018). The deposit's total volume, however, is proportional to the deposited amount, i.e. broadly the same in these experiments irrespective of deposition method. Indeed, it was by building on these assumptions that the evaporation model succeeded in reproducing the observations in Fig. 4. With the much smaller surface area of the syringe deposited material, it requires more time to evaporate all the PEG-8 than from the equivalent amount of deposited aerosol particles. This time delay directly translates to a shift to higher observed  $T_{max}$  values. The desorption model mimics this change in surface-to-volume ratio by increasing the initial size of the modelled evaporating particle to 1.3  $\mu\text{m}$  and 11  $\mu\text{m}$ . But note that there are no individual spherical particles of that size on the filter.

### 3.3. Particle size and heating ramp rate effect in atomizer method

265 As  $T_{max}$  values have been reported to vary in aerosol measurements (Huang et al., 2018; Schobesberger et al., 2018), we investigated how different particle sizes and FIGAERO heating ramp rates influence the measured  $T_{max}$  values with the atomizer method.

We performed measurements with PEG mixture aerosol particles with monodisperse mobility sizes of 80 nm and 300 nm and 270 mass loadings in between 150-170 ng, while using a ramping time of 15 min (Figure 7 panel a). Note that  $T_{max}$  results differ from results shown in Sect. 3.1 due to different FIGAERO inlet used here. Monodisperse particles showed a consistent difference in measured  $T_{max}$  of  $\sim 7$  °C between 80 nm and 300 nm particles for all PEGs, which translates to roughly half an order of magnitude difference when used to calibrate the  $C^*$  space. Our evaporation model confirms this difference for all PEGs except PEG-8. The difference between different particle sizes can be explained with different surface-to-volume ratios 275 as was discussed in the previous section.

We observed a difference of 3-5 °C in measured  $T_{max}$  values between heating ramp times of 15 min (11.4 K min<sup>-1</sup>) and 30 min (6.25 K min<sup>-1</sup>) (Figure 7 panel b). The evaporation model yields the same difference between the two heating times, even though actual  $T_{max}$  values are slightly overestimated. The difference in observed  $T_{max}$  values between different ramping rates 280 is expected. With a slower linear ramping rate, for example, more time will have passed at any momentary desorption temperature, allowing a larger fraction of molecules to have already evaporated. Consequently, the supply of molecules will become exhausted at a lower desorption temperature, which causes the peak that defines  $T_{max}$ .

An additional aspect that has been reported to shift  $T_{max}$  values is the amount of collected aerosol mass on the PTFE filter (Huang et al., 2018), becoming important when collected particulate mass is around several micrograms. We tested the mass loading effect by collecting different amounts of atomized PEG's up to 200 ng of mass and found no clear difference between measured  $T_{max}$  values (data not shown). However, as collected aerosol mass on the FIGAERO filter can easily reach microgram

amounts, especially when sampling in highly polluted environments and as we did not rigorously test how  $T_{max}$  values behave above 200 ng, we suggest that this effect is investigated further in future publications.

### 290 3.4. Sensitivity calibration comparison

The syringe deposition method has often been used to calibrate the sensitivity of the FIGAERO particle phase measurements, i.e. to correlate the number of measured ions to the collected material on the filter (Lopez-Hilfiker et al., 2014; Liu et al., 2016). These measurements are typically done in a similar way as described in Sect 2.2 but varying the amount of deposited calibrant by varying the amount of deposited solution. The signal of the calibration compound is then integrated over the full heating  
295 period and contrasted against the deposited mass after which a linear fit yields the instrument's sensitivity.

In Figure 8 we compare the sensitivity calibration for PEG-7, done with the syringe deposition method (blue), to equivalent measurements, done with atomized monodisperse particles instead (green). The results of the two methods are in excellent agreement, which confirms the feasibility of the atomizer method also in sensitivity calibrations. However, when using the  
300 atomizer method in sensitivity calibrations, additional precautions should be taken to ensure that all assumptions made in the mass loading calculations are valid. For example, possible particle agglomeration must be considered when atomizing high particle number concentrations, in particular when using compounds that form solid particles at room temperature and at RH prior to FIGAERO sampling, such as ammonium sulphate or citric acid. As agglomerated solid particles are generally not spherical, as is often assumed for mass loading calculations, calculated particle mass loading on the filter can be overestimated.  
305 We therefore recommend using the syringe deposition method for sensitivity calibrations, also because the amount of required instrumentation and associated errors are much smaller.

### 3.5 $P_{sat}$ of higher order PEGs

As  $T_{max}$  values of the used PEGs only reach up to  $\sim 80$  °C, but  $T_{max}$  values of ambient aerosols are reported as high as 160 °C (Huang et al., 2019), it would be beneficial to extend the calibration range to higher  $T_{max}$  values for more accurate calibrations.  
310 PEGs are commercially available in polymer lengths of more than 30 chains, but unfortunately available saturation pressure data only extends up to PEG-8 (Krieger et al., 2018). However, as PEGs are straight chain polymers, it could be assumed that  $\log(P_{sat})$  of higher order PEGs increase in a linear fashion, which is also suggested in Krieger et al., 2018. We include results of  $T_{max}$  measurements using higher-order PEGs (up to PEG-16) and two tentative analysis approaches via estimating the  $P_{sat}$  value of those compounds in the SI Sect. S4.

### 315 3.6 Impact of using different calibration methods

Figure 9 panels a) and b) show Volatility Basis Set (VBS) distributions constructed from FIGAERO desorption measurements of SOA. formed from photo-oxidation of  $\alpha$ -pinene in a flow tube experiment. A more detailed description of the SOA production is shown in Ylisirniö et al., 2020. We used  $T_{max}$  to  $P_{sat}$  calibration coefficients acquired either via the atomizer

method or via the syringe method, in the latter case with a solution concentration of 0.01 g L<sup>-1</sup> standard solution depositions.

320 ~~A more detailed description of the SOA production is shown in Ylisirniö et al., 2020. Note that the calibrations shown in this paper used faster heating ramp rates than what was used in the SOA measurements. Note that the heating ramp rates in these calibrations were done with faster heating ramp rate than in the SOA measurements,~~ introducing an overall small systematic error (<1 order of magnitude in  $C^*$  space) towards higher saturation concentrations. However, the presented differences are unaffected. The used calibration curves are shown in panel c) and panel d) reproduces the calibration lines of Fig. 9c, but in  
325 terms of  $C^*$  for a compound with ~~molecular weight~~molar mass of 200 g mol<sup>-1</sup>.

Results clearly demonstrate the effect of using the syringe deposition method versus the atomization method. When using the calibration coefficients from the atomizer method, there is a shift towards lower volatilities: the amount of Low Volatile Organic Compounds (LVOC) and Extremely Low Organic Compounds (ELVOC) is increased, while Semi Volatile Organic  
330 Compounds (SVOC) compounds mostly disappear. The magnitude of this shift is presented more directly, albeit approximately, in Fig. 9d. The difference in  $C^*$  between the two calibration methods is ~1 order of magnitude at 50 °C, increasing to ~2.5 orders of magnitude at 100 °C.

The difference is strong enough to have the potential to change the aerosol growth dynamics in global climate models  
335 employing VBS distributions and could thus impact the estimation of Cloud Condensation Nuclei (CCN) numbers which in turn leads to an underestimation of the reflected solar radiation from clouds (Sporre et al., 2020).

#### 4 Summary and Conclusions

In this study we introduced an improved method for FIGAERO-CIMS volatility calibration from peak thermogram value  $T_{max}$   
340 to saturation pressure  $P_{sat}$ , by atomizing the used calibration compounds and compared the results to the thus far more often used syringe deposition method. With the syringe deposition method, we found a clear effect of solution concentration on measured  $T_{max}$  values (e.g., Fig. 3). This effect can lead to severe overestimation of saturation vapor pressure values when derived from measured  $T_{max}$ . For investigating those differences in calibration results, we also employed evaporation modelling and took direct Scanning Electron Microscope pictures of calibration compounds deposited onto the FIGAERO filter. Both  
345 the modelling and SEM images shows that the structure and the volume of the deposited unit controls the evaporation. Syringe deposited calibration compounds form patches of material when the solvent evaporates, whereas collected aerosol particles stay as separate particles on the filter. The atomized particles have much higher surface-to-volume ratio compared to the syringe deposited patches and so a similar total amount of deposit will evaporate more quickly from the filter. As the FIGAERO inlet is designed to measure ambient aerosol particles, it stands to reason that using atomizer method will yield more  
350 appropriate calibration results than the syringe deposition method.

In Fig. S2 we show again previously reported calibration lines shown in Fig. 1, now updated with calibration lines acquired in this study with both the atomizer (solid green line) and the syringe method (conc.  $0.1 \text{ g L}^{-1}$ , solid blue line). The area between the two solid lines encompasses almost all other reported calibration lines. It should be noted that even though the calibration lines extend all the way to  $200 \text{ }^{\circ}\text{C}$ ,  $T_{max}$  values used for the fitting are below  $120 \text{ }^{\circ}\text{C}$  in almost all the studies.

To explore possible uncertainties in the atomizer method due to sensitivities to experimental settings, we also investigated the effect of particle size and heating ramp rate to the measured  $T_{max}$  values. We found overall differences of  $\sim 7 \text{ K}$  between  $80 \text{ nm}$  and  $300 \text{ nm}$  PEG particles and of  $\sim 3 \text{ K}$  between  $15 \text{ min}$  and  $30 \text{ min}$  ramp rates. These differences translate to roughly half order of magnitude change in saturation concentration ( $C^*$ ) space. As the used particle size has a moderate impact on the measured  $T_{max}$  values, it is advisable to use polydisperse aerosol for calibration with particle size distributions close to the actual aerosol size distribution that is being measured.

We also tested how the atomizer method performs against the syringe deposition method in sensitivity calibrations with using PEG-7 as calibrant compound. The two methods produced practically identical sensitivity calibration curves when using liquid aerosol particles. However, possible measurement errors and infrastructure requirements for the atomizer method may make the syringe deposition method more feasible for sensitivity calibrations.

We finally compared how the use of calibration curves from the two methods impact the VBS distribution derived from SOA formed from photo-oxidation of  $\alpha$ -pinene. We found that using calibration parameters from the atomizer method shifted the VBS distribution  $\sim 1$ - $3$  orders of magnitude compared to the VBS distribution derived with the syringe deposition method, especially increasing the amount of LVOC and ELVOC compounds. This shift is strong enough to affect our understanding and modelling results of SOA formation and dynamics and ultimately, how these processes are treated in global climate models, potentially affecting calculated CCN values.

An essential aspect of calibrating the  $T_{max}$ - $P_{sat}$  relationship for FIGAERO is the use of reference  $P_{sat}$  values for the calibration compounds. As we pointed out in the introduction, the  $P_{sat}$  values found in the literature for typical organic compounds have high variations depending on the literature source (see Table S1). Therefore we strongly recommend that FIGAERO-CIMS  $T_{max}$  to  $P_{sat}$  calibrations should be performed using atomized PEGs, with literature  $P_{sat}$  values currently being reported in Krieger et al., 2018. We note that these  $P_{sat}$  values have not been verified by other studies and are subject to corrections, but want to point out that harmonizing further FIGAERO calibrations by using PEGs would make future FIGAERO measurements more comparable to each other. For example, volatility datasets derived from FIGAERO measurements using an atomized PEG-based calibration could be corrected with minimum efforts if more accurate  $P_{sat}$  values for PEG became available, or if the available set of  $P_{sat}$  values was extended to higher order PEGs.

*Data availability.* The data shown in the paper is available on request from corresponding author.

390 *Author contributions.* AY and SS led the paper writing, AY, LB and IP made the measurements. All co-authors participated in the interpretation of the results and paper editing.

*Competing interests.* Jordan Krechmer, John Jayne, and Douglas Worsnop work for Aerodyne Research, Inc., which commercialized the FIGAERO inlet.

395 *Acknowledgements.* We thank Jari Leskinen from SIB Labs facilities for assistance in SEM imaging.

*Financial support.* This research was supported by the Academy of Finland (272041, 310682, 299544) and the University of Eastern Finland Doctoral Program in Environmental Physics, Health and Biology.

## 400 **References**

- Bannan, T. J., Le Breton, M., Priestley, M., Worrall, S. D., Bacak, A., Marsden, N. A., Mehra, A., Hammes, J., Hallquist, M., Alfarra, M. R., Krieger, U. K., Reid, J. P., Jayne, J., Robinson, W., McFiggans, G., Coe, H., Percival, C. J. and Topping, D.: A method for extracting calibrated volatility information from the FIGAERO-HR-ToF-CIMS and its experimental application, *Atmos. Meas. Tech.*, 12(3), 1429–1439, doi:10.5194/amt-12-1429-2019, 2019.
- 405 Le Breton, M., Wang, Y., Hallquist, A. M., Kant Pathak, R., Zheng, J., Yang, Y., Shang, D., Glasius, M., Bannan, T. J., Liu, Q., Chan, C. K., Percival, C. J., Zhu, W., Lou, S., Topping, D., Wang, Y., Yu, J., Lu, K., Guo, S., Hu, M. and Hallquist, M.: Online gas- and particle-phase measurements of organosulfates, organosulfonates and nitrooxy organosulfates in Beijing utilizing a FIGAERO ToF-CIMS, *Atmos. Chem. Phys.*, 18(14), 10355–10371, doi:10.5194/acp-18-10355-2018, 2018.
- 410 Le Breton, M., Psichoudaki, M., Hallquist, M., Watne, K., Lutz, A. and Hallquist, M.: Application of a FIGAERO ToF CIMS for on-line characterization of real-world fresh and aged particle emissions from buses, *Aerosol Sci. Technol.*, 53(3), 244–259, doi:10.1080/02786826.2019.1566592, 2019.
- Cappa, C. D., Lovejoy, E. R. and Ravishankara, A. R.: Determination of evaporation rates and vapor pressures of very low volatility compounds: A study of the C4-C10 and C 12 dicarboxylic acids, *J. Phys. Chem. A*, 111(16), 3099–3109, doi:10.1021/jp068686q, 2007.
- 415 D’Ambro, E. L., Lee, B. H., Liu, J., Shilling, J. E., Gaston, C. J., Lopez-Hilfiker, F. D., Schobesberger, S., Zaveri, R. A., Mohr, C., Lutz, A., Zhang, Z., Gold, A., Surratt, J. D., Rivera-Rios, J. C., Keutsch, F. N. and Thornton, J. A.: Molecular composition and volatility of isoprene photochemical oxidation secondary organic aerosol under low- and high-NO<sub>x</sub> conditions, *Atmos. Chem. Phys.*, 17(1), 159–174,

doi:10.5194/acp-17-159-2017, 2017.

Donahue, N. M., Kroll, J. H., Pandis, S. N. and Robinson, A. L.: A two-dimensional volatility basis set-Part 2: Diagnostics of organic-aerosol evolution, *Atmos. Chem. Phys.*, 12(2), 615–634, doi:10.5194/acp-12-615-2012, 2012.

420 Eichler, P., Müller, M., D’Anna, B. and Wisthaler, A.: A novel inlet system for online chemical analysis of semi-volatile submicron particulate matter, *Atmos. Meas. Tech.*, 8(3), 1353–1360, doi:10.5194/amt-8-1353-2015, 2015.

Hallquist, M., Wenger, J. C., Baltensperger, U., Rudich, Y., Simpson, D., Claeys, M., Dommen, J., Donahue, N. M., George, C., Goldstein, a. H., Hamilton, J. F., Herrmann, H., Hoffmann, T., Iinuma, Y., Jang, M., Jenkin, M. E., Jimenez, J. L., Kiendler-Scharr, a., Maenhaut, W., McFiggans, G., Mentel, T. F., Monod, a., Prévôt, a. S. H., Seinfeld, J. H., Surratt, J. D., Szmigielski, R. and Wildt, J.: The formation, properties and impact of secondary organic aerosol: current and emerging issues, *Atmos. Chem. Phys.*, 9(14), 5155–5236, doi:10.5194/acp-9-5155-2009, 2009.

425 Hong, J., Äijälä, M., Häme, S. A. K., Hao, L., Duplissy, J., Heikkinen, L. M., Nie, W., Mikkilä, J., Kulmala, M., Prisle, N. L., Virtanen, A., Ehn, M., Paasonen, P., Worsnop, D. R., Riipinen, I., Petäjä, T. and Kerminen, V. M.: Estimates of the organic aerosol volatility in a boreal forest using two independent methods, *Atmos. Chem. Phys.*, 17(6), 4387–4399, doi:10.5194/acp-17-4387-2017, 2017.

430 Huang, W., Saathoff, H., Pajunoja, A., Shen, X., Naumann, K. H., Wagner, R., Virtanen, A., Leisner, T. and Mohr, C.:  $\alpha$ -Pinene secondary organic aerosol at low temperature: Chemical composition and implications for particle viscosity, *Atmos. Chem. Phys.*, 18(4), 2883–2898, doi:10.5194/acp-18-2883-2018, 2018.

Huang, W., Saathoff, H., Shen, X., Ramisetty, R., Leisner, T. and Mohr, C.: Seasonal characteristics of organic aerosol chemical composition and volatility in Stuttgart, Germany, *Atmos. Chem. Phys.*, 19(18), 11687–11700, doi:10.5194/acp-19-11687-2019, 2019.

435 Isaacman-Vanwertz, G., Massoli, P., O’Brien, R., Lim, C., Franklin, J. P., Moss, J. A., Hunter, J. F., Nowak, J. B., Canagaratna, M. R., Misztal, P. K., Arata, C., Roscioli, J. R., Herndon, S. T., Onasch, T. B., Lambe, A. T., Jayne, J. T., Su, L., Knopf, D. A., Goldstein, A. H., Worsnop, D. R. and Kroll, J. H.: Chemical evolution of atmospheric organic carbon over multiple generations of oxidation, *Nat. Chem.*, 10(4), 462–468, doi:10.1038/s41557-018-0002-2, 2018.

440 Iyer, S., He, X., Hyttinen, N., Kurtén, T. and Rissanen, M. P.: Computational and Experimental Investigation of the Detection of HO<sub>2</sub> Radical and the Products of Its Reaction with Cyclohexene Ozonolysis Derived RO<sub>2</sub> Radicals by an Iodide-Based Chemical Ionization Mass Spectrometer, *J. Phys. Chem. A*, 121(36), 6778–6789, doi:10.1021/acs.jpca.7b01588, 2017.

445 Jimenez, J. L., Canagaratna, M. R., Donahue, N. M., Prevot, A. S. H., Zhang, Q., Kroll, J. H., DeCarlo, P. F., Allan, J. D., Coe, H., Ng, N. L., Aiken, A. C., Docherty, K. S., Ulbrich, I. M., Grieshop, A. P., Robinson, A. L., Duplissy, J., Smith, J. D., Wilson, K. R., Lanz, V. A., Hueglin, C., Sun, Y. L., Tian, J., Laaksonen, A., Raatikainen, T., Rautiainen, J., Vaattovaara, P., Ehn, M., Kulmala, M., Tomlinson, J. M., Collins, D. R., Cubison, M. J., Dunlea, E. J., Huffman, J. A., Onasch, T. B., Alfarra, M. R., Williams, P. I., Bower, K., Kondo, Y., Schneider, J., Drewnick, F., Borrmann, S., Weimer, S., Demerjian, K., Salcedo, D., Cottrell, L., Griffin, R., Takami, A., Miyoshi, T., Hatakeyama, S., Shimono, A., Sun, J. Y., Zhang, Y. M., Dzepina, K., Kimmel, J. R., Sueper, D., Jayne, J. T., Herndon, S. C., Trimborn, A. M., Williams, L. R., Wood, E. C., Middlebrook, A. M., Kolb, C. E., Baltensperger, U. and Worsnop, D. R.: Evolution of organic aerosols in the atmosphere, *Science* (80-. ), 326(5959), 1525–1529, doi:10.1126/science.1180353, 2009.

450 Joo, T., Rivera-Rios, J. C., Takeuchi, M., Alvarado, M. J. and Ng, N. L.: Secondary Organic Aerosol Formation from Reaction of 3-Methylfuran with Nitrate Radicals, *ACS Earth Sp. Chem.*, 3(6), 922–934, doi:10.1021/acsearthspacechem.9b00068, 2019.

455 Krieger, U. K., Siegrist, F., Marcolli, C., Emanuelsson, E. U., Gøbel, F. M., Bilde, M., Marsh, A., Reid, J. P., Huisman, A. J., Riipinen, I., Hyttinen, N., Myllys, N., Kurtén, T., Bannan, T., Percival, C. J. and Topping, D.: A reference data set for validating vapor pressure measurement techniques: Homologous series of polyethylene glycols, *Atmos. Meas. Tech.*, 11(1), 49–63, doi:10.5194/amt-11-49-2018, 2018.

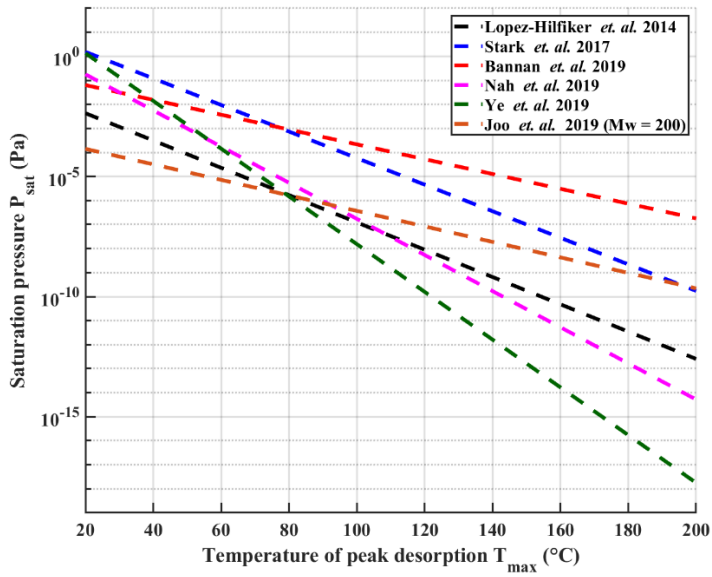
Lee, B. H., Lopez-Hilfiker, F. D., Mohr, C., Kurtén, T., Worsnop, D. R. and Thornton, J. A.: An iodide-adduct high-resolution time-of-flight chemical-ionization mass spectrometer: Application to atmospheric inorganic and organic compounds, *Environ. Sci. Technol.*, 48(11), 6309–6317, doi:10.1021/es500362a, 2014.

Li, Z., Tikkanen, O. P., Buchholz, A., Hao, L., Kari, E., Yli-Juuti, T. and Virtanen, A.: Effect of Decreased Temperature on the Evaporation

- 460 of  $\alpha$ -Pinene Secondary Organic Aerosol Particles, *ACS Earth Sp. Chem.*, 3(12), 2775–2785, doi:10.1021/acsearthspacechem.9b00240, 2019.
- Liu, J., D'Ambro, E. L., Lee, B. H., Lopez-Hilfiker, F. D., Zaveri, R. A., Rivera-Rios, J. C., Keutsch, F. N., Iyer, S., Kurten, T., Zhang, Z., Gold, A., Surratt, J. D., Shilling, J. E. and Thornton, J. A.: Efficient Isoprene Secondary Organic Aerosol Formation from a Non-IEPOX Pathway, *Environ. Sci. Technol.*, 50(18), 9872–9880, doi:10.1021/acs.est.6b01872, 2016.
- Lopez-Hilfiker, F. D., Mohr, C., Ehn, M., Rubach, F., Kleist, E., Wildt, J., Mentel, T. F., Lutz, A., Hallquist, M., Worsnop, D. and Thornton, J. A.: A novel method for online analysis of gas and particle composition: Description and evaluation of a filter inlet for gases and AEROSols (FIGAERO), *Atmos. Meas. Tech.*, 7(4), 983–1001, doi:10.5194/amt-7-983-2014, 2014.
- 465 Mikkonen, S., Pitkänen, M. R. A., Nieminen, T., Lipponen, A., Isokääntä, S., Arola, A. and Lehtinen, K. E. J.: Technical note: Effects of Uncertainties and Number of Data points on Inference from Data &ndash; a Case Study on New Particle Formation, *Atmos. Chem. Phys.*, 19(19), 12531–12543, doi:https://doi.org/10.5194/acp-19-12531-2019, 2019.
- 470 Mohr, C., Thornton, J. A., Heitto, A., Lopez-Hilfiker, F. D., Lutz, A., Riipinen, I., Hong, J., Donahue, N. M., Hallquist, M., Petäjä, T., Kulmala, M. and Yli-Juuti, T.: Molecular identification of organic vapors driving atmospheric nanoparticle growth, *Nat. Commun.*, 10(1), 1–7, doi:10.1038/s41467-019-12473-2, 2019.
- Nah, T., Xu, L., Osborne-Benthaus, K. A., White, S. M., France, S. and Lee Ng, N.: Mixing order of sulfate aerosols and isoprene epoxydiols affects secondary organic aerosol formation in chamber experiments, *Atmos. Environ.*, 217(August), doi:10.1016/j.atmosenv.2019.116953, 475 2019.
- Pitkänen, M. R. A., Mikkonen, S., Lehtinen, K. E. J., Lipponen, A. and Arola, A.: Artificial bias typically neglected in comparisons of uncertain atmospheric data, *Geophys. Res. Lett.*, 43(18), 10,003-10,011, doi:10.1002/2016GL070852.1., 2016.
- Riva, M., Heikkinen, L., Bell, D. M., Peräkylä, O., Zha, Q., Schallhart, S., Rissanen, M. P., Imre, D., Petäjä, T., Thornton, J. A., Zelenyuk, A. and Ehn, M.: Chemical transformations in monoterpene-derived organic aerosol enhanced by inorganic composition, *npj Clim. Atmos. Sci.*, 2(1), 1–9, doi:10.1038/s41612-018-0058-0, 2019.
- 480 Schobesberger, S., D'Ambro, E. L., Lopez-Hilfiker, F. D., Mohr, C. and Thornton, J. A.: A model framework to retrieve thermodynamic and kinetic properties of organic aerosol from composition-resolved thermal desorption measurements, *Atmos. Chem. Phys.*, 18(20), 14757–14785, doi:10.5194/acp-18-14757-2018, 2018.
- Smith, J. N., Moore, K. F., McMurry, P. H. and Eisele, F. L.: Atmospheric Measurements of Sub-20 nm Diameter Particle Chemical Composition by Thermal Desorption Chemical Ionization Mass Spectrometry, *Aerosol Sci. Technol.*, 38(2), 100–110, doi:10.1080/02786820490249036, 2004.
- 485 Sporre, M. K., Blichner, S. M., Schrödner, R., Karset, I. H. H., Berntsen, T. K., Noije, T. Van, Bergman, T., Donnell, D. O. and Makkonen, R.: Large difference in aerosol radiative effects from BVOC-SOA treatment in three ESMs, , (February), 1–38, 2020.
- Stark, H., Yatavelli, R. L. N., Thompson, S. L., Kang, H., Krechmer, J. E., Kimmel, J. R., Palm, B. B., Hu, W., Hayes, P. L., Day, D. A., Campuzano-Jost, P., Canagaratna, M. R., Jayne, J. T., Worsnop, D. R. and Jimenez, J. L.: Impact of Thermal Decomposition on Thermal Desorption Instruments: Advantage of Thermogram Analysis for Quantifying Volatility Distributions of Organic Species, *Environ. Sci. Technol.*, 51(15), 8491–8500, doi:10.1021/acs.est.7b00160, 2017.
- 490 Stolzenburg, D., Fischer, L., Vogel, A. L., Heinritzi, M., Schervish, M., Simon, M., Wagner, A. C., Dada, L., Ahonen, L. R., Amorim, A., Baccarini, A., Bauer, P. S., Baumgartner, B., Bergen, A., Bianchi, F., Breitenlechner, M., Brilke, S., Mazon, S. B., Chen, D., Dias, A., Draper, D. C., Duplissy, J., Haddad, I. El, Finkenzeller, H., Frege, C., Fuchs, C., Garmash, O., Gordon, H., He, X., Helm, J., Hofbauer, V., Hoyle, C. R., Kim, C., Kirkby, J., Kontkanen, J., Kürten, A., Lampilahti, J., Lawler, M., Lehtipalo, K., Leiminger, M., Mai, H., Mathot, S., Mentler, B., Molteni, U., Nie, W., Nieminen, T., Nowak, J. B., Ojdanic, A., Onnela, A., Passananti, M., Petäjä, T., Quéléver, L. L. J., Rissanen, M. P., Sarnela, N., Schallhart, S., Tauber, C., Tomé, A., Wagner, R., Wang, M., Weitz, L., Wimmer, D., Xiao, M., Yan, C., Ye, P., Zha, Q., Baltensperger, U., Curtius, J., Dommen, J., Flagan, R. C., Kulmala, M., Smith, J. N., Worsnop, D. R., Hansel, A., Donahue, N. M. and Winkler, P. M.: Rapid growth of organic aerosol nanoparticles over a wide tropospheric temperature range, *Proc. Natl. Acad. Sci. U. S. A.*, 115(37), 9122–9127, doi:10.1073/pnas.1807604115, 2018.
- 500 Wang, M., Chen, D., Xiao, M., Ye, Q., Stolzenburg, D., Hofbauer, V., Ye, P., Vogel, A. L., Mauldin, R. L., Amorim, A., Baccarini, A.,

- 505 Baumgartner, B., Brilke, S., Dada, L., Dias, A., Duplissy, J., Finkenzeller, H., Garmash, O., He, X. C., Hoyle, C. R., Kim, C., Kvashnin, A., Lehtipalo, K., Fischer, L., Molteni, U., Petäjä, T., Pospisilova, V., Quéléver, L. L. J., Rissanen, M., Simon, M., Tauber, C., Tomé, A., Wagner, A. C., Weitz, L., Volkamer, R., Winkler, P. M., Kirkby, J., Worsnop, D. R., Kulmala, M., Baltensperger, U., Dommen, J., El-Haddad, I. and Donahue, N. M.: Photo-oxidation of Aromatic Hydrocarbons Produces Low-Volatility Organic Compounds, *Environ. Sci. Technol.*, 54(13), 7911–7921, doi:10.1021/acs.est.0c02100, 2020.
- Yatavelli, R. L. N. and Thornton, J. a.: Particulate Organic Matter Detection Using a Micro-Orifice Volatilization Impactor Coupled to a Chemical Ionization Mass Spectrometer (MOVI-CIMS), *Aerosol Sci. Technol.*, 44(1), 61–74, doi:10.1080/02786820903380233, 2010.
- 510 Ye, Q., Wang, M., Hofbauer, V., Stolzenburg, D., Chen, D., Schervish, M., Vogel, A., Mauldin, R. L., Baalbaki, R., Brilke, S., Dada, L., Dias, A., Duplissy, J., El Haddad, I., Finkenzeller, H., Fischer, L., He, X., Kim, C., Kürten, A., Lamkaddam, H., Lee, C. P., Lehtipalo, K., Leiminger, M., Manninen, H. E., Marten, R., Mentler, B., Partoll, E., Petäjä, T., Rissanen, M., Schobesberger, S., Schuchmann, S., Simon, M., Tham, Y. J., Vazquez-Pufleau, M., Wagner, A. C., Wang, Y., Wu, Y., Xiao, M., Baltensperger, U., Curtius, J., Flagan, R., Kirkby, J., Kulmala, M., Volkamer, R., Winkler, P. M., Worsnop, D. and Donahue, N. M.: Molecular Composition and Volatility of Nucleated Particles
- 515 from  $\alpha$ -Pinene Oxidation between  $-50\text{ }^{\circ}\text{C}$  and  $+25\text{ }^{\circ}\text{C}$ , *Environ. Sci. Technol.*, 53(21), 12357–12365, doi:10.1021/acs.est.9b03265, 2019.
- Yli-Juuti, T., Pajunoja, A., Tikkanen, O. P., Buchholz, A., Faiola, C., Väisänen, O., Hao, L., Kari, E., Peräkylä, O., Garmash, O., Shiraiwa, M., Ehn, M., Lehtinen, K. and Virtanen, A.: Factors controlling the evaporation of secondary organic aerosol from  $\alpha$ -pinene ozonolysis, *Geophys. Res. Lett.*, 44(5), 2562–2570, doi:10.1002/2016GL072364, 2017.
- 520 Ylisirniö, A., Buchholz, A., Mohr, C., Li, Z., Barreira, L., Lambe, A., Faiola, C., Kari, E., Yli-Juuti, T., Nizkorodov, S. A., Worsnop, D. R., Virtanen, A. and Schobesberger, S.: Composition and volatility of secondary organic aerosol (SOA) formed from oxidation of real tree emissions compared to simplified volatile organic compound (VOC) systems, *Atmos. Chem. Phys.*, 20(9), 5629–5644, doi:10.5194/acp-20-5629-2020, 2020.
- York, D., Evensen, N. M., Martínez, M. L. and De Basabe Delgado, J.: Unified equations for the slope, intercept, and standard errors of the best straight line, *Am. J. Phys.*, 72(3), 367–375, doi:10.1119/1.1632486, 2004.

525



530 Figure 1. Previously reported calibration measurements with temperature at peak desorption ( $T_{max}$ ) plotted against saturation  
 535 pressure  $P_{sat}$ . The Joo *et al.*, (2019) line has been converted from saturation concentration values to saturation pressure assuming a  
molecular mass of 200. All lines except Joo *et al.*, (2019) are also refitted from literature data using the fitting routine  
 described in Sect. 2.5. It is notable that in most cases the data points used for the fitting do not reach  $T_{max}$  values higher than 120 °C,  
 which is likely partially responsible for the further-large divergence of results when extrapolating to higher  $T_{max}$ . Error bars of the  
fits are omitted for sake of clarity.

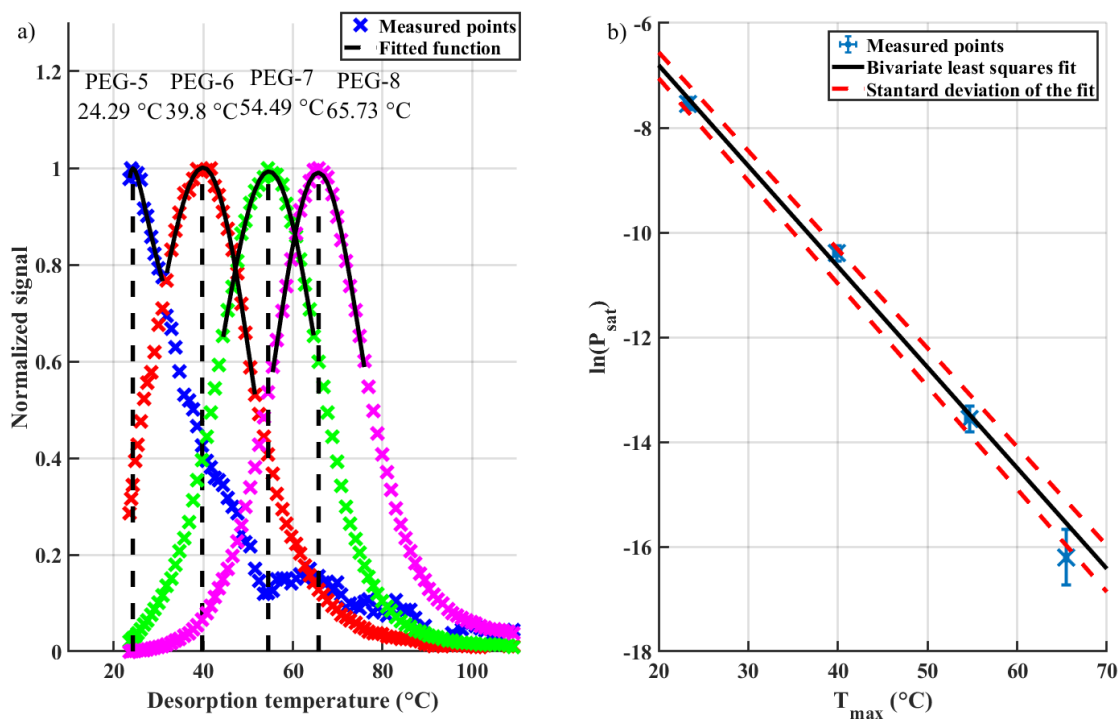
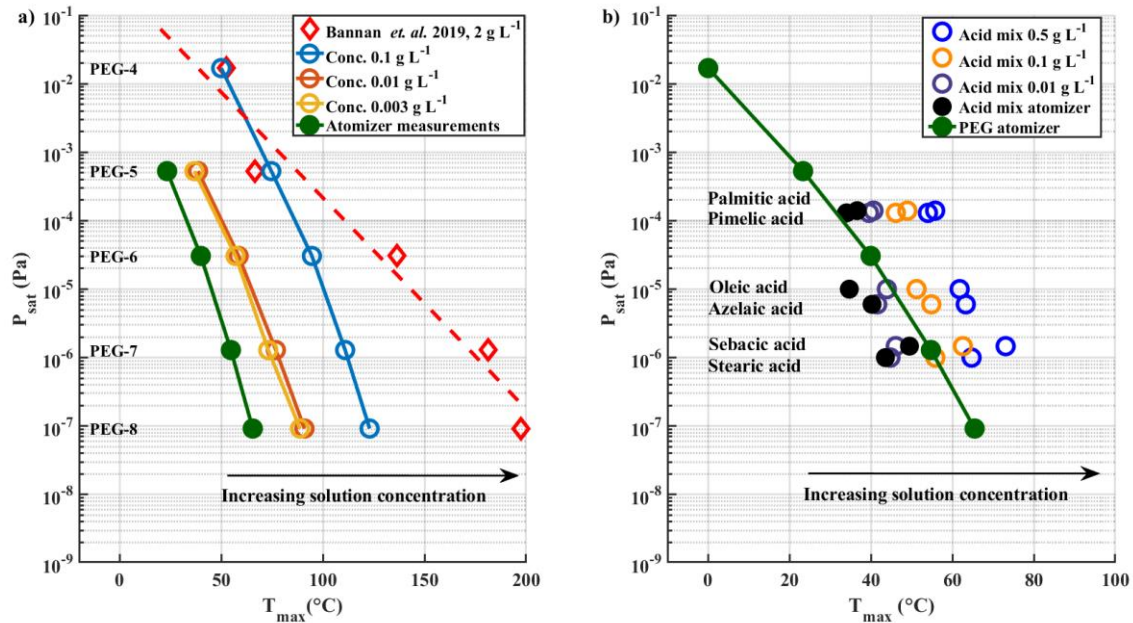


Figure 2. Panel a) example for acquiring  $T_{max}$  values from thermograms with fitted asymmetric lognormal function. Panel b) Fitting a line to the natural logarithm of literature-based saturation vapor pressures ( $P_{sat}$ , in units of Pa) as a function of corresponding FIGAERO-derived  $T_{max}$  values, while taking the uncertainties into account. With  $P_{sat}$ , uncertainties are taken from the literature and with  $T_{max}$ , the uncertainties are defined as the standard deviation of three measurements. Fitting parameters of the line fit were  $a = -0.1923 \pm 0.0039$  and  $b = -2.9589 \pm 0.17$ .

540



545 | Figure 3. Solution concentration effect. Literature-based saturation vapour pressure  $P_{sat}$  are plotted vs. measured  $T_{max}$  for a) PEG compounds and b) carboxylic acids with a logarithmic y-axis. Black arrows in both panels indicate the direction of shift in  $T_{max}$  values as the solution concentration increases. PEG atomizer results are also included in panel b) for reference.

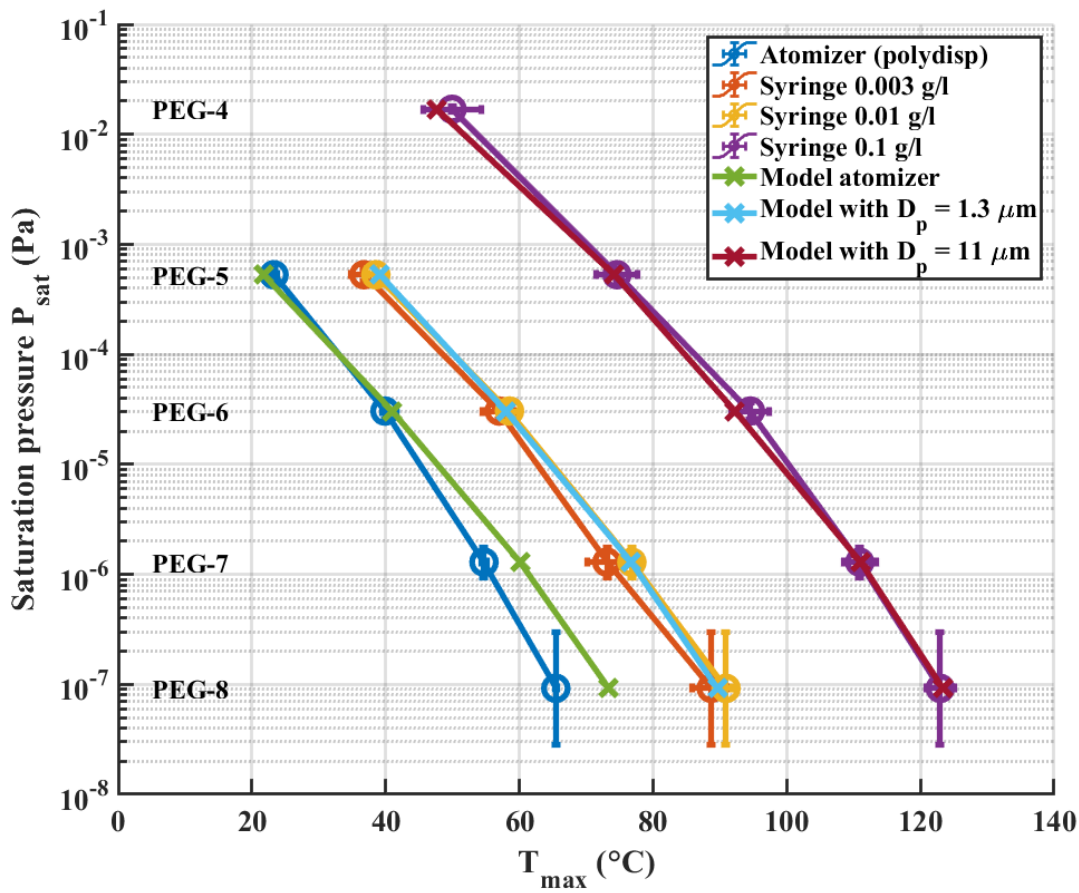


Figure 4. Comparison of the solution concentration effect on PEG results with model results. Error bars in  $T_{max}$  values are standard deviations of three repetitions.

550

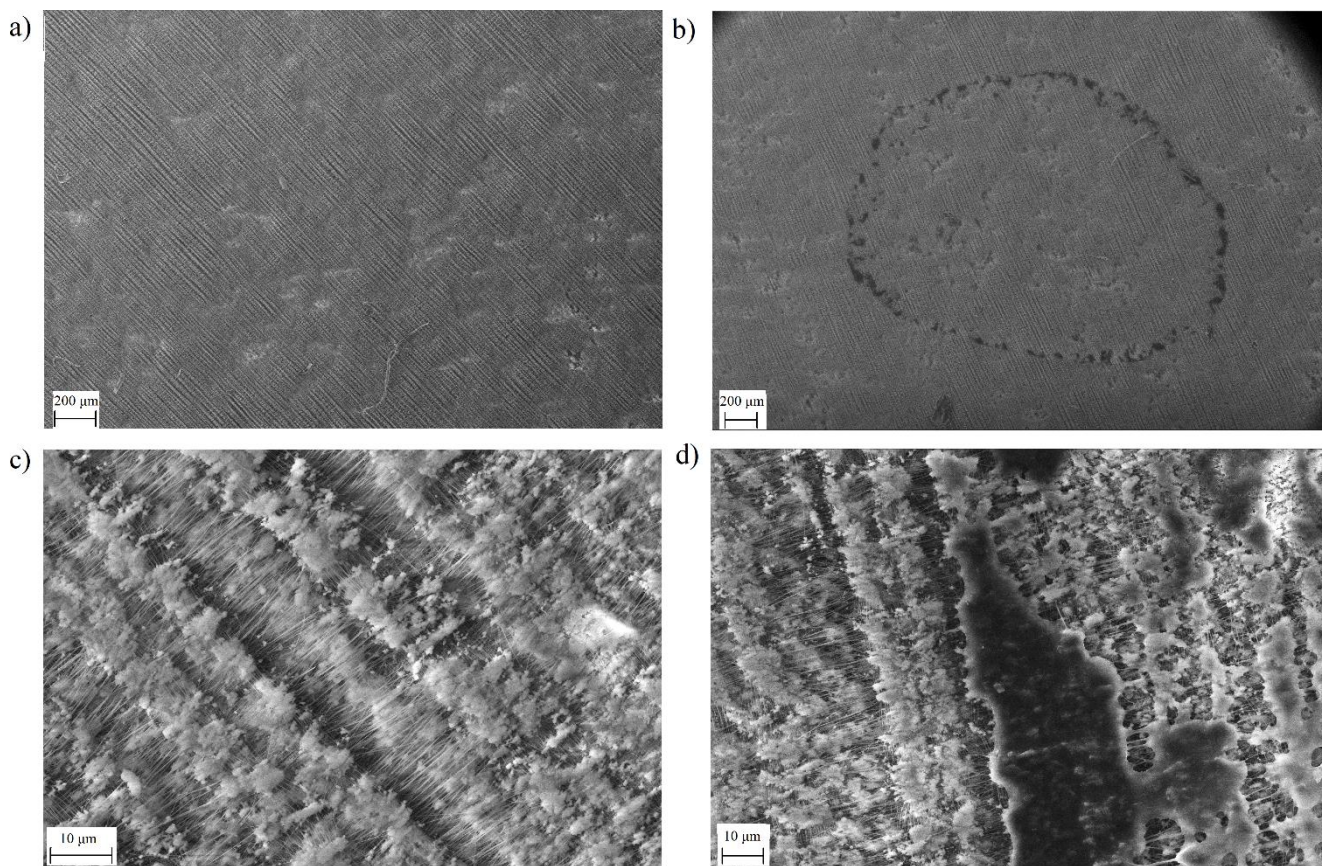
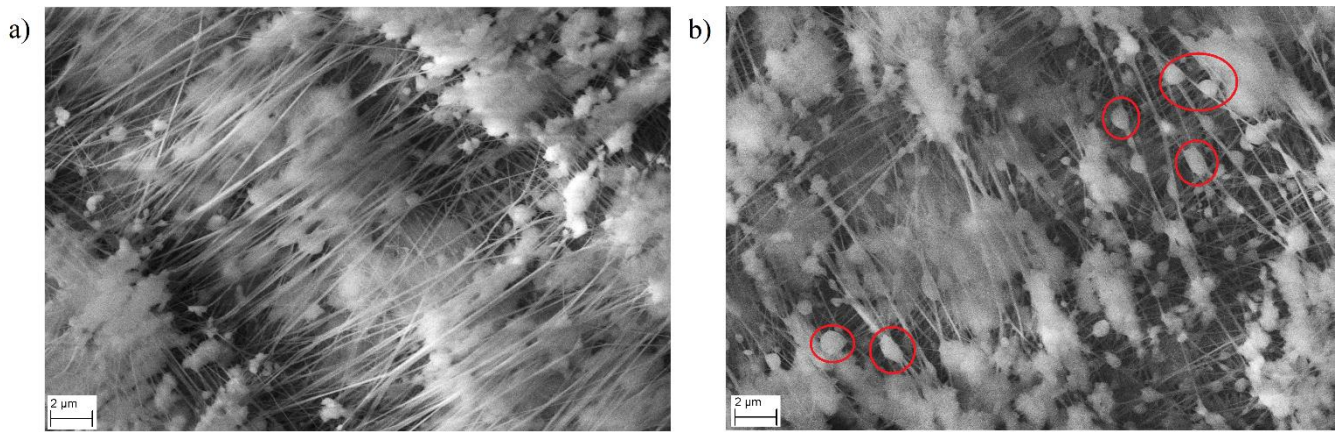


Figure 5. SEM pictures. Panel a) 10  $\mu\text{l}$  of pure ACN deposited on the filter. Panel b) 3  $\mu\text{l}$  of PEG-8 with concentration of  $0.01 \text{ g L}^{-1}$  (30 ng) in ACN deposited on the filter. Panel c) magnification shows magnification panel a) and panel d) shows magnification of the PEG-8 residue. Panel e) magnification of the edge of the PEG-8 “ring”.

555



560 **Figure 6. SEM pictures. Panel a) magnification of a clean FIGAERO filter with no collected particles. Panel b) a magnification of a FIGAERO filter with collected 300 nm sized PEG-8 particles. Red circles in panel b) emphasize selected spots where liquid PEG-8 particles are deposited.**

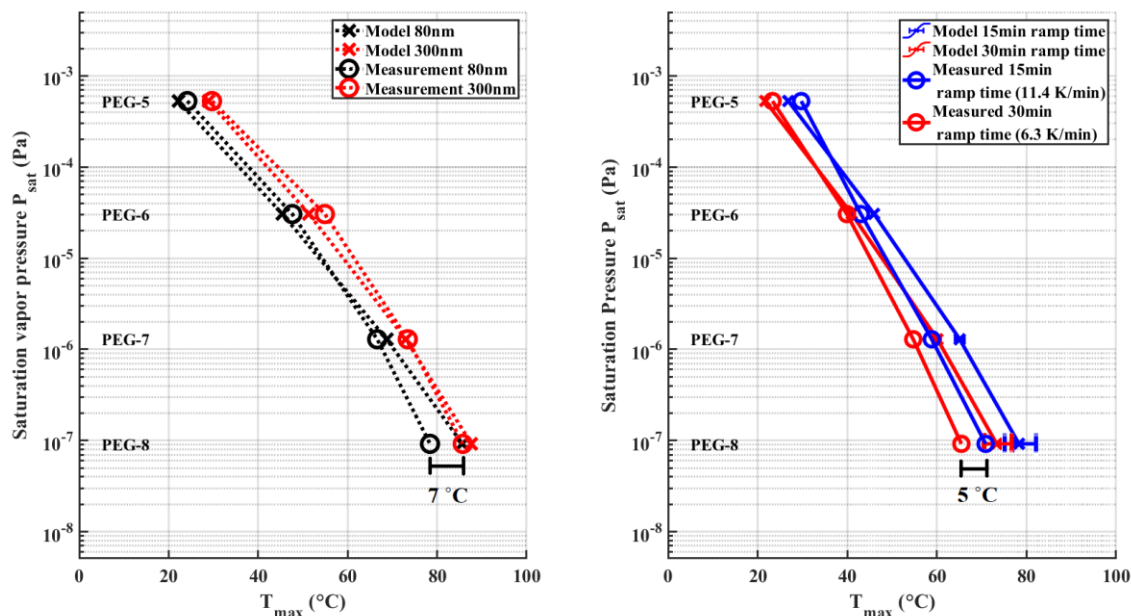


Figure 7. a)  $T_{max}$  values measured for 80 nm and 300 nm particles with ramp time of 15 min. The difference in  $T_{max}$  between the two particles sizes is  $\sim 7^\circ\text{C}$ . Panel b) shows measured  $T_{max}$  values of 15 min and 30 min ramping times using polydisperse aerosol particles. The difference between the two heating rates is  $\sim 5^\circ\text{C}$ . Error bars are omitted from the measured values in the figure for sake of clarity. In the panel b) whiskers show the range of model results when using uncertainties of evaporation enthalpy shown in (Krieger et al., (2018)). The standard deviations of the for all measured points is panel a) is between  $0.2\text{--}0.5^\circ\text{C}$ . In panel b) the standard deviations for measured points are between  $0.2\text{--}1.3^\circ\text{C}$ .

565

570

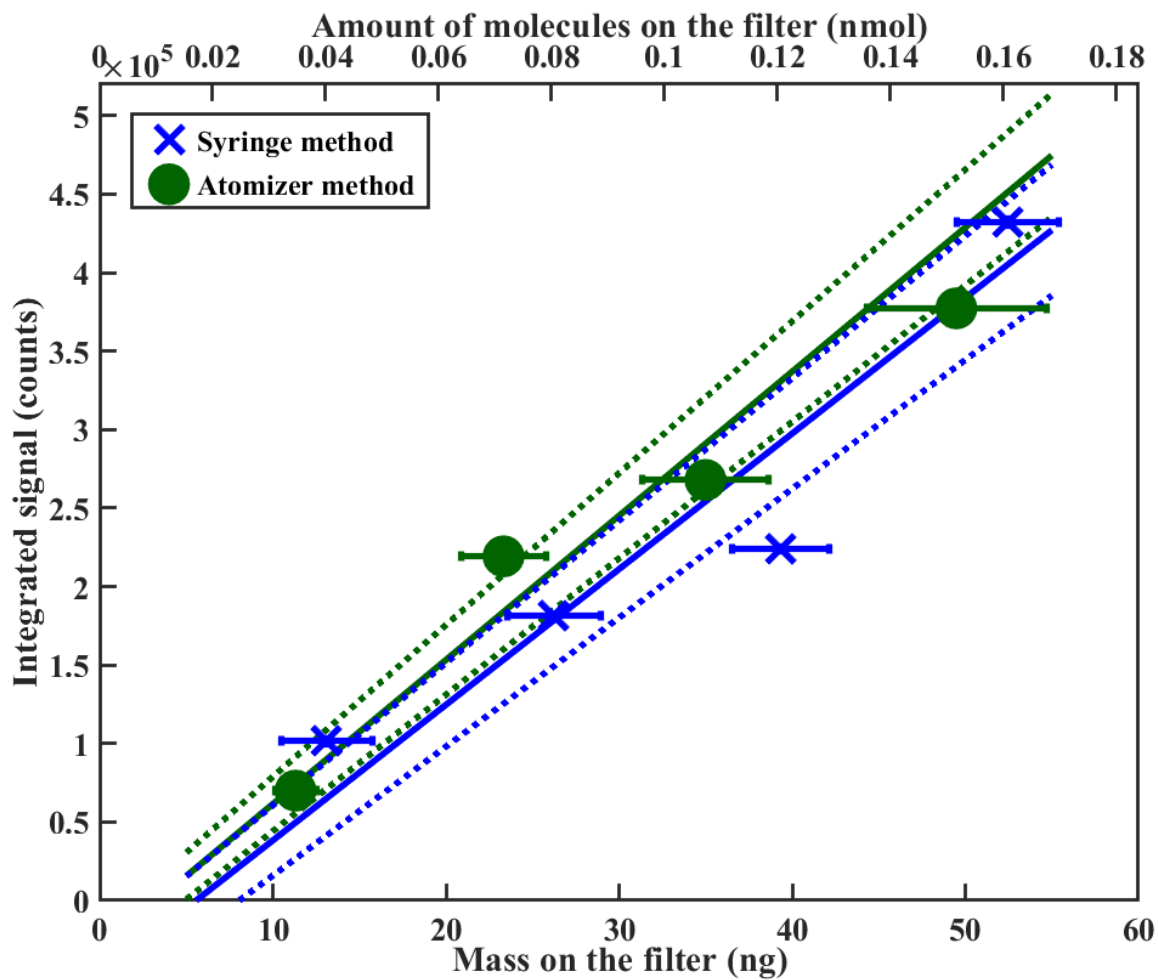


Figure 8. Sensitivity comparison between different calibration methods using PEG-7. The bottom x-axis shows the deposited mass on the filter; the top x-axis shows the same amount in nano moles. Note that y-axis error bars are too small to be seen in the figure. Further explanation of the error analysis is shown in the SI

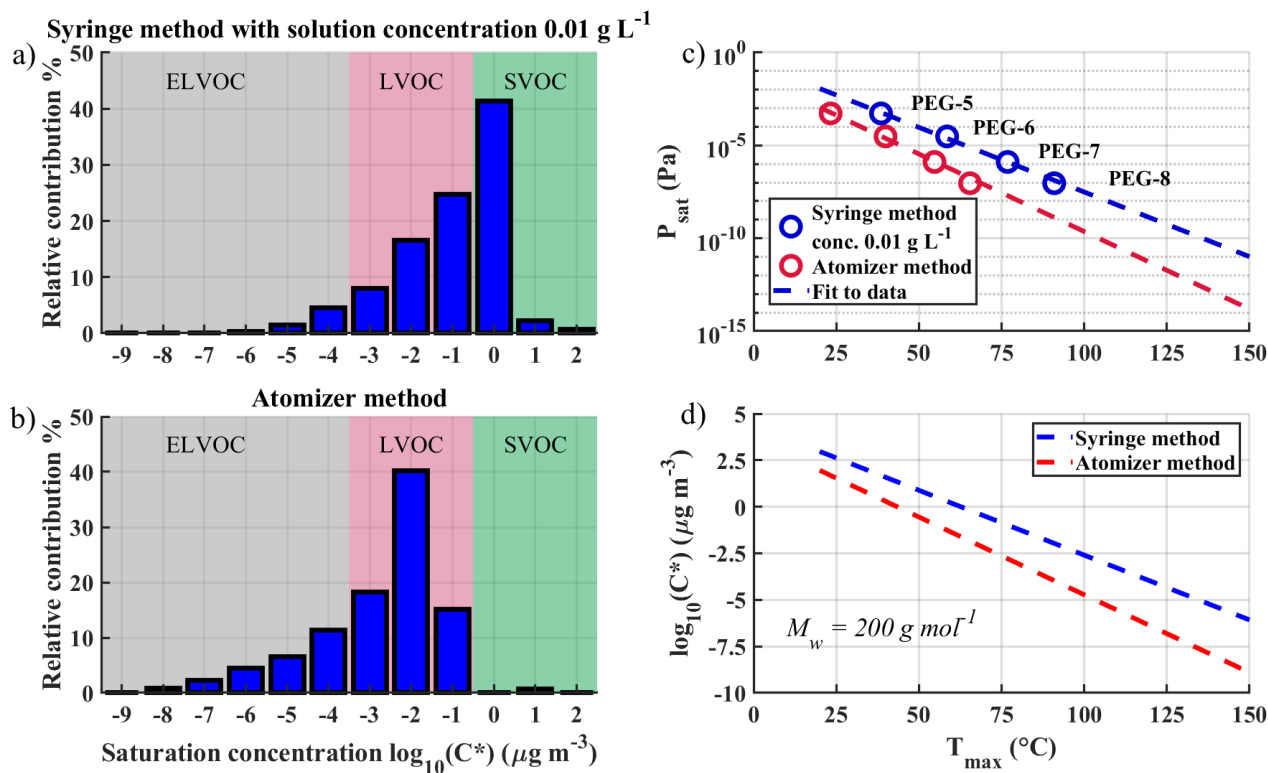


Figure 9. Comparison of volatility basis sets (VBS) derived for the same SOA but using different calibration methods. Panel a) shows VBS determined with deposition method and panel b) shows VBS determined with atomizer method using the same data set. The respectively used calibration lines are shown in panel c). Panel d) shows how different calibration lines would impact the log<sub>10</sub>(C\*) value of a compound with  $M_w$  of 200 g mol<sup>-1</sup> with different  $T_{max}$  values.

1 Supplement information for  
 2 Ylisirniö et. al. AMT-2020-254

3

4 S1. Different  $P_{sat}$  values used in FIGAERO-ToF-CIMS calibrations in different studies

5

6 *Table S1. Collection of literature-based  $P_{sat}$  (Pa) values used in various published FIGAERO*  
 7 *calibrations.  $P_{sat}$  values used in this study are taken from (Lopez-Hilfiker et al., (2014)).*

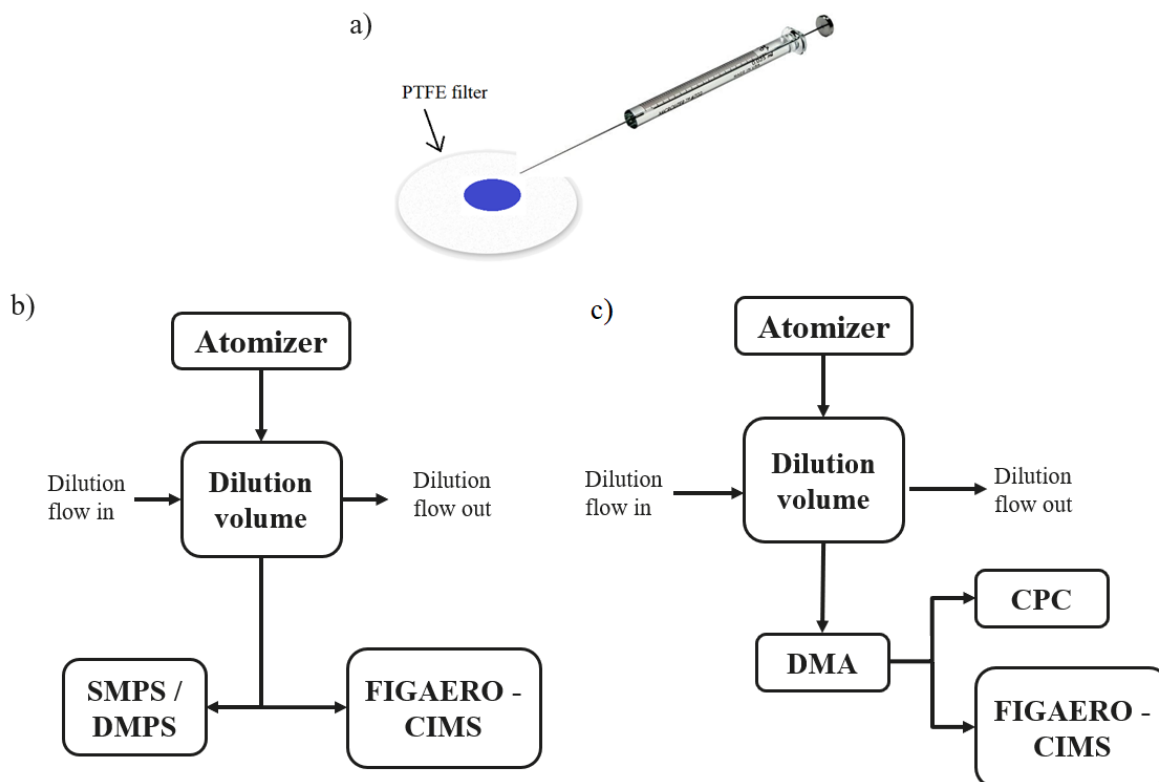
Saturation pressure (Pa)	Lopez-Hilfiker et al., (2014)	Stark et al., (2017)	Nah et al., (2019)	Bannan et al., (2019)	Ye et al., (2019)	(Wang et al., 2020)	This study
Glutaric acid		$6.7 \times 10^{-4}$	$1 \times 10^{-3}$	$1 \times 10^{-3}$	$4 \times 10^{-4}$	$2.6 \times 10^{-4}$	
Cis-Pinonic acid	$6 \times 10^{-5}$	0.03	$7.8 \times 10^{-4}$	$7.79 \times 10^{-4}$			
Pimelic acid	$1.3 \times 10^{-4}$		$2.6 \times 10^{-4}$				$1.3 \times 10^{-4}$
Erythritol			$6.3 \times 10^{-5}$				
Palmitic acid	$1.4 \times 10^{-4}$		$2.0 \times 10^{-5}$		$5 \times 10^{-5}$	$2.8 \times 10^{-5}$	$1.4 \times 10^{-4}$
Azelaic acid	$6 \times 10^{-6}$	$6 \times 10^{-6}$	$7.4 \times 10^{-6}$			$1.4 \times 10^{-6}$	$6 \times 10^{-6}$
Oleic acid	$1 \times 10^{-6}$						
Stearic acid	$1 \times 10^{-5}$		$2.5 \times 10^{-6}$				$1 \times 10^{-6}$
Sebacic acid	$1.5 \times 10^{-6}$		$1.5 \times 10^{-6}$				$1.5 \times 10^{-6}$
Behenic acid	$7 \times 10^{-4}$		$4.9 \times 10^{-8}$				
Oleic acid	$1 \times 10^{-5}$						$1 \times 10^{-5}$
Tricarballic acid		$3 \times 10^{-7}$			$3.1 \times 10^{-7}$	$3.1 \times 10^{-7}$	
Pinic acid	$6 \times 10^{-5}$	$4.3 \times 10^{-5}$		$3.2 \times 10^{-5}$	$9.3 \times 10^{-5}$		
Citric acid					$2.7 \times 10^{-10}$	$2.7 \times 10^{-10}$	
Camphoric acid					$2 \times 10^{-4}$	$2 \times 10^{-5}$	
Dodecanoic/lauric acid					0.01		
Succinic acid				$1.3 \times 10^{-3}$			
Malonic acid				$6.2 \times 10^{-4}$			
Adipic acid				$1.8 \times 10^{-4}$			
Suberic acid				$2.23 \times 10^{-5}$			

8

9

10

11 S2. Measurement schematics



12  
 13 *Figure S1. Panel a) illustration of the syringe deposition method. Measurement setup schematics for*  
 14 *the atomizer method either with b) polydisperse particles or c) monodisperse particles. The dilution*  
 15 *volume is used in the atomizer method to ensure complete evaporation of the solvent before particle*  
 16 *characterization.*

17  
 18 S3. Measured  $T_{max}$  values

19  
 20 *Table S2. Average  $T_{max}$  values ( $^{\circ}\text{C}$ ) and standard deviations based on three repetitions, as shown in*  
 21 *Figure 3 panel a). Used  $P_{sat}$  (Pa), based on Krieger et al., (2018), are shown in the bottom row.*

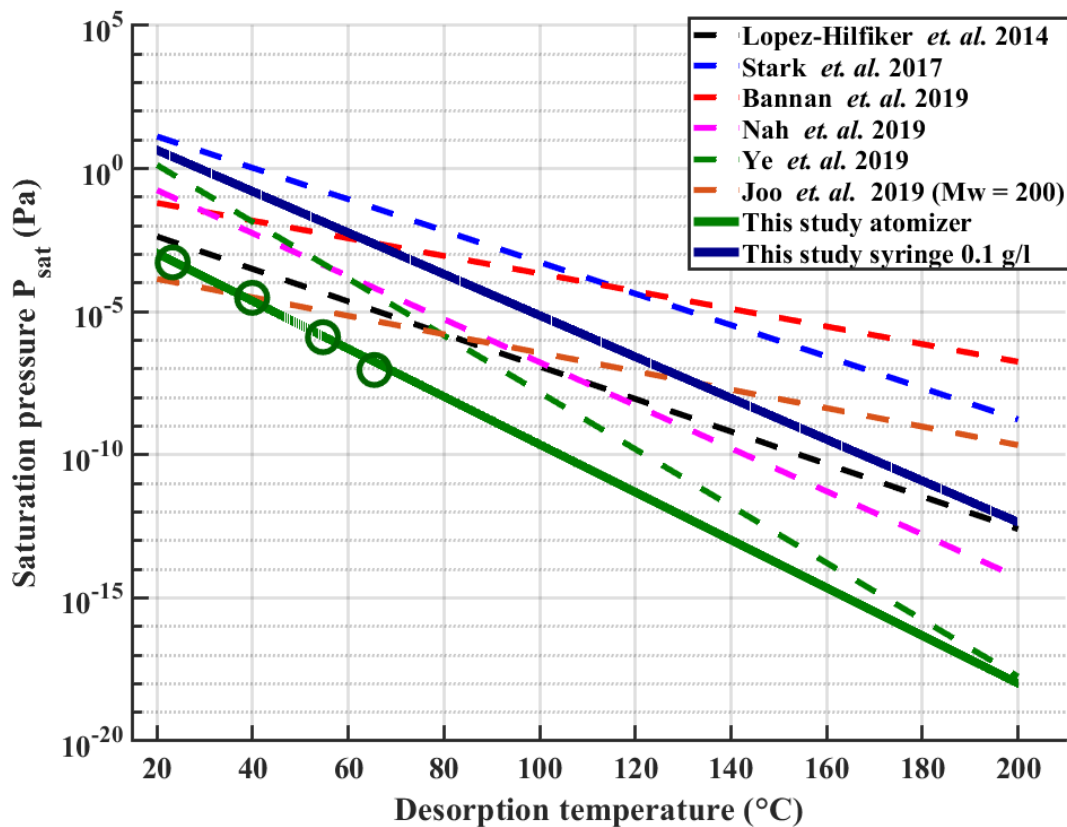
Experiment	PEG-4	PEG-5	PEG-6	PEG-7	PEG-8
Conc. 0.1 g L <sup>-1</sup>	49.9±4.4	74.6 ± 3.1	94.6 ± 2.8	110.9 ± 2.4	123 ± 2
Conc. 0.01 g L <sup>-1</sup>		38.5 ± 1.2	58.5 ± 1.5	76.8 ± 1.2	90.9 ± 0.9
Conc. 0.003 g L <sup>-1</sup>		36.7 ± 1.9	57 ± 2.5	73.1 ± 2.9	88.7 ± 2.8
Atomizer		23.3 ± 0.5	39.9 ± 0.4	54.7 ± 0.4	65.5 ± 0.2
Saturation pressure (Pa)	0.0169	5.29 x 10 <sup>-4</sup>	3.05 x 10 <sup>-5</sup>	1.29 x 10 <sup>-6</sup>	9.2 x 10 <sup>-8</sup>

22  
 23  
 24

25 Table S3. Average  $T_{max}$  values ( $^{\circ}\text{C}$ ) and standard deviations based on three repetitions, as shown in  
 26 Figure 3 panel b). Used saturation pressure (Pa) values are shown in the bottom row.

Experiment	Palmitic acid	Pimelic acid	Oleic acid	Azelaic acid	Stearic acid	Sebacic acid
Conc. 0.5 g L <sup>-1</sup>	55.8 ± 0.3	54 ± 0.1	61.8 ± 2.8	63.3 ± 0.3	64.7 ± 0.5	73.1 ± 0.1
Conc. 0.1 g L <sup>-1</sup>	48.9 ± 1	46.1 ± 1.1	51.2 ± 1.8	54.8 ± 1.2	55.8 ± 1	62.6 ± 1.2
Conc. 0.01 g L <sup>-1</sup>	40.6 ± 1.2	39.5 ± 2	43.9 ± 2.8	41.5 ± 1.5	44.8 ± 2.5	46.1 ± 0.4
Atomizer	36.6 ± 0.6	34 ± 0.4	34.7 ± 0.8	40.2 ± 0.7	43.5 ± 0.6	49.4 ± 1
Saturation pressure (Pa)	1.4 x 10 <sup>-4</sup>	1.3 x 10 <sup>-4</sup>	1 x 10 <sup>-5</sup>	6 x 10 <sup>-6</sup>	1 x 10 <sup>-6</sup>	1.47 x 10 <sup>-6</sup>

27



28

29 Figure S2. Repeated Fig. 1 (dashed lines) with calibration lines from this study added for the atomizer  
 30 method (green solid line) and the syringe method (for a solution concentration of 0.1 g L<sup>-1</sup>, solid blue  
 31 line). Both lines are for 30 min ramping times and the atomizer measurements used polydisperse aerosol  
 32 with a median particle size of 60 nm. Green circles show the measured data where the line have been  
 33 fitted.

34

35 S4. Error analysis for Figure 8.

36

37 Errors for deposited mass on the filter shown in Fig.8 are determined with propagation of error for  
38 both methods. For syringe deposition the equation is of the form

39 
$$m_{syringe} = V_s C_s$$

40 where  $V_s$  (ml) is the injected volume and  $C_s$  ( $g\ l^{-1}$ ) is the mass concentration of the solution. The  
41 solution was prepared by weighting the analyte with a microscale and solving it to 200 ml of ACN to  
42 make 0.2 g/l solution. The stock solution was then diluted into 50ml solution of 0.01 g/l  
43 concentration. To account for the dilution, the equation now becomes to form

44 
$$m_{syringe} = \frac{V_{syr} V_{pip}}{V_{fin} V_{sto}} m_{scale}$$

45 where  $V_{syr}$  is deposited volume to the filter,  $V_{pip}$  is volume pipetted from stock solution to make the  
46 dilute solution,  $V_{fin}$  is the volume final dilute solution,  $V_{sto}$  is the volume of the stock solution and  
47  $m_{scale}$  is the analytes mass measured with the microscale. Now denoting

48 
$$R = \frac{V_{syr} V_{pip}}{V_{fin} V_{sto}}$$

49 we get the equation to the form

50 
$$m_{syr} = R m_{scale}$$

51 and formula for propagation of error becomes

52 
$$\Delta m_{syringe} = \sqrt{\left(\frac{\partial m_{syr}}{\partial R}\right)^2 \Delta R^2 + \left(\frac{\partial m_{syr}}{\partial m_{scale}}\right)^2 \Delta m_{scale}^2}$$

53 
$$\Delta m_{syringe} = \sqrt{m_{scale}^2 \Delta R^2 + R^2 \Delta m_{scale}^2}$$

54 where

55 
$$\Delta R = \sqrt{\left(\frac{V_{pip}}{V_{fin} V_{sto}}\right)^2 \Delta V_{syr}^2 + \left(\frac{V_{syr}}{V_{fin} V_{sto}}\right)^2 \Delta V_{pip}^2 + \left(-\frac{V_{syr} V_{pip}}{V_{fin}^2 V_{sto}}\right)^2 \Delta V_{fin}^2 + \left(-\frac{V_{syr} V_{pip}}{V_{fin} V_{sto}^2}\right)^2 \Delta V_{sto}^2}$$

56 When using Class A glassware, tolerances for different measurement flasks can be found online.

57

58 Atomizer deposition

59 Amount of deposited particulate mass can be calculated with equation

60 
$$m_{atom} = FtV_c$$

61 where  $F$  is the flow through the filter [ $m^3\ s^{-1}$ ],  $t$  [s] is the collection time and  $V_c$  [ $\mu g\ m^{-3}$ ] is the particle  
62 mass concentration in the sample air. The propagation of error formula for this equation is of the form

63 
$$\Delta m_{atom} = \sqrt{\left(\frac{\partial m_{atom}}{\partial F}\right)^2 \Delta F^2 + \left(\frac{\partial m_{atom}}{\partial t}\right)^2 \Delta t^2 + \left(\frac{\partial m_{atom}}{\partial V_c}\right)^2 \Delta V_c^2}$$

64 
$$\Delta m_{atom} = \sqrt{(tV_c)^2 \Delta F^2 + (FV_c)^2 \Delta t^2 + (Ft)^2 \Delta V_c^2}$$

65

66 where  $\Delta F = 0.01 \times F$  (flow meter accuracy),  $\Delta t = 1$  (assuming swift movement of the tray). When  
67 using monodisperse aerosol sampling method as shown in Fig. S1 b), particle mass concentration can  
68 be calculated by assuming spherical particle shape as

$$69 \quad V_c = \frac{\rho d_p^3 \pi n}{6},$$

70 where  $\rho$  is the density of the aerosol particles,  $d_p$  is the set monodisperse particle size and  $n$  is  
71 particle number concentration measured with CPC. The uncertainty of  $V_c$  is then

$$72 \quad \Delta V_c = \sqrt{\left(\frac{3\rho d_p^2 \pi}{6}\right)^2 \Delta d_p^2 + \left(\frac{\rho d_p^3 \pi}{6}\right)^2 \Delta n^2},$$

73 where  $\Delta d_p = 0.01 \times d_p$  and  $\Delta n = 0.1 \times n$  with instrumentation described in Sect. 2.4.

74

75 Y-axis errors for Figure 8 are calculated by assuming Poisson-type measurement error for CIMS  
76 measurements (Yan et al., 2016)

$$77 \quad e_i = \sqrt{\frac{S_i}{\Delta t} + a},$$

78 where  $S_i$  is the measured signal,  $\Delta t$  is the difference of two-time steps and  $a$  is constant accounting for  
79 electrical noise.

80 When integrating over such data, we assumed error to be of the form

$$81 \quad \Delta I = \pm 1.96 \sqrt{\text{std}(S)^2 + \sum e_i^2},$$

82 where  $\text{std}(S)$  is the standard deviation over the whole thermogram.

83

#### 84 S4S5. $P_{sat}$ of higher order PEGs

85

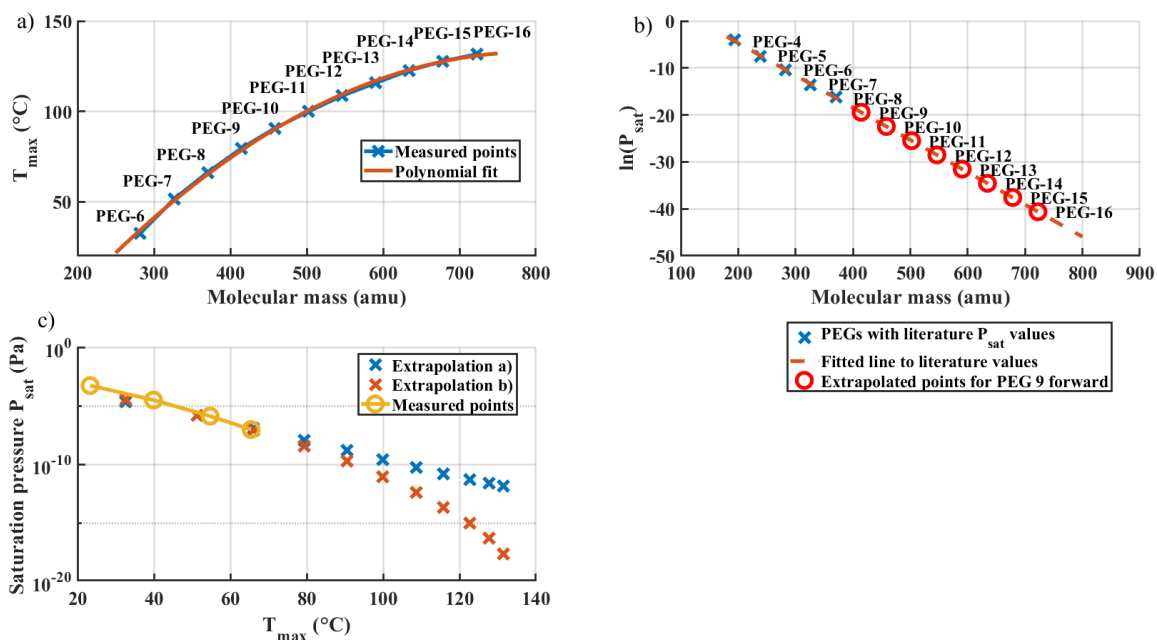
86 We performed additional  $T_{max}$  measurements of an atomized PEG-400 solution (Sigma Aldrich),  
87 which contains different PEGs so that the average molecular mass of the solution is about 400 g/mol.  
88 Detected PEGs ranged from PEG-6 to PEG-16. Fig. S3 a) shows measured  $T_{max}$  values of different  
89 PEGs versus the molecular mass of the compounds. The measured points follow well a second order  
90 polynomial fitted to the points. It should be noted that  $T_{max}$  values of PEG-400 are about 5-7 °C higher  
91 than values measured for individual PEGs, possibly due to additional stabilization compounds in the  
92 product. Figure S3 b) shows a somewhat bold log-linear extrapolation of saturation pressures from  
93 measured PEGs (4-8) up to PEG-16.

94

95 In Fig S3 c) we show two extrapolations for  $P_{sat}$  vs. measured  $T_{max}$ . Extrapolation a) was done by  
96 substituting  $T_{max}$  values in eq. (2) with the polynomial fit to molecular mass ( $T_{max} = d Mw^2 + e Mw +$   
97  $f$ , where  $Mw$  is molecular weight and  $d$ ,  $e$  and  $f$  are fitted constants), shown in Fig. S3a, while using  
98 fit coefficients  $a$  and  $b$  from eq. (2). I.e., extrapolation a) estimates  $P_{sat}$  values based on molecular

99 mass. Extrapolation b) was done by directly fitting the normal logarithm of  $P_{sat}$  vs molecular mass  
100 (Fig. S3 b).

101  
102 As can be seen, the two extrapolation methods for  $P_{sat}$  lead to substantially different extended  
103 calibration curves in the higher desorption temperatures. Our results anyhow strongly suggest that  
104 higher order PEGs could be used for extending the volatility calibration range, if their saturation  
105 vapor pressures were established by accurate independent measurements or estimated with high  
106 enough certainty.



107  
108 *Figure S3. Panel a) measured  $T_{max}$  values (crosses) vs. molecular mass of the PEGs contained in the*  
109 *PEG-400 mixture, and a polynomial fit applied to the data. Panel b) natural logarithm of saturation*  
110 *pressure vs. PEG molecular mass, and a linear fit to the literature-supported data sub-set (crosses),*  
111 *extrapolated to extend to all other PEGs (circles). Panel c) saturation pressure  $P_{sat}$  vs  $T_{max}$  extrapolated*  
112 *to cover all PEG, using extrapolations based on the fitted functions in panels a) and b).*

113

## 114 References

115

116 Bannan, T. J., Le Breton, M., Priestley, M., Worrall, S. D., Bacak, A., Marsden, N. A., Mehra, A.,  
117 Hammes, J., Hallquist, M., Alfarra, M. R., Krieger, U. K., Reid, J. P., Jayne, J., Robinson, W.,  
118 McFiggans, G., Coe, H., Percival, C. J. and Topping, D.: A method for extracting calibrated volatility  
119 information from the FIGAERO-HR-ToF-CIMS and its experimental application, *Atmos. Meas.*  
120 *Tech.*, 12(3), 1429–1439, doi:10.5194/amt-12-1429-2019, 2019.

121 Krieger, U. K., Siegrist, F., Marcolli, C., Emanuelsson, E. U., Gøbel, F. M., Bilde, M., Marsh, A.,  
122 Reid, J. P., Huisman, A. J., Riipinen, I., Hyttinen, N., Myllys, N., Kurtén, T., Bannan, T., Percival, C.  
123 J. and Topping, D.: A reference data set for validating vapor pressure measurement techniques:  
124 Homologous series of polyethylene glycols, *Atmos. Meas. Tech.*, 11(1), 49–63, doi:10.5194/amt-11-  
125 49-2018, 2018.

126 Lopez-Hilfiker, F. D., Mohr, C., Ehn, M., Rubach, F., Kleist, E., Wildt, J., Mentel, T. F., Lutz, A.,  
127 Hallquist, M., Worsnop, D. and Thornton, J. A.: A novel method for online analysis of gas and  
128 particle composition: Description and evaluation of a filter inlet for gases and AEROSols  
129 (FIGAERO), *Atmos. Meas. Tech.*, 7(4), 983–1001, doi:10.5194/amt-7-983-2014, 2014.

130 Nah, T., Xu, L., Osborne-Benthaus, K. A., White, S. M., France, S. and Lee Ng, N.: Mixing order of  
131 sulfate aerosols and isoprene epoxydiols affects secondary organic aerosol formation in chamber  
132 experiments, *Atmos. Environ.*, 217(August), doi:10.1016/j.atmosenv.2019.116953, 2019.

133 Stark, H., Yatavelli, R. L. N., Thompson, S. L., Kang, H., Krechmer, J. E., Kimmel, J. R., Palm, B.  
134 B., Hu, W., Hayes, P. L., Day, D. A., Campuzano-Jost, P., Canagaratna, M. R., Jayne, J. T., Worsnop,  
135 D. R. and Jimenez, J. L.: Impact of Thermal Decomposition on Thermal Desorption Instruments:  
136 Advantage of Thermogram Analysis for Quantifying Volatility Distributions of Organic Species,  
137 *Environ. Sci. Technol.*, 51(15), 8491–8500, doi:10.1021/acs.est.7b00160, 2017.

138 Wang, M., Chen, D., Xiao, M., Ye, Q., Stolzenburg, D., Hofbauer, V., Ye, P., Vogel, A. L., Mauldin,  
139 R. L., Amorim, A., Baccarini, A., Baumgartner, B., Brilke, S., Dada, L., Dias, A., Duplissy, J.,  
140 Finkenzeller, H., Garmash, O., He, X. C., Hoyle, C. R., Kim, C., Kvashnin, A., Lehtipalo, K., Fischer,  
141 L., Molteni, U., Petäjä, T., Pospisilova, V., Quéléver, L. L. J., Rissanen, M., Simon, M., Tauber, C.,  
142 Tomé, A., Wagner, A. C., Weitz, L., Volkamer, R., Winkler, P. M., Kirkby, J., Worsnop, D. R.,  
143 Kulmala, M., Baltensperger, U., Dommen, J., El-Haddad, I. and Donahue, N. M.: Photo-oxidation of  
144 Aromatic Hydrocarbons Produces Low-Volatility Organic Compounds, *Environ. Sci. Technol.*,  
145 54(13), 7911–7921, doi:10.1021/acs.est.0c02100, 2020.

146 Yan, C., Nie, W., Aijälä, M., Rissanen, M. P., Canagaratna, M. R., Massoli, P., Junninen, H., Jokinen,  
147 T., Sarnela, N., Häme, S. A. K., Schobesberger, S., Canonaco, F., Yao, L., Prévôt, A. S. H., Petäjä, T.,  
148 Kulmala, M., Sipilä, M., Worsnop, D. R. and Ehn, M.: Source characterization of highly oxidized  
149 multifunctional compounds in a boreal forest environment using positive matrix factorization, *Atmos.*  
150 *Chem. Phys.*, 16(19), 12715–12731, doi:10.5194/acp-16-12715-2016, 2016.

151 Ye, Q., Wang, M., Hofbauer, V., Stolzenburg, D., Chen, D., Schervish, M., Vogel, A., Mauldin, R. L.,  
152 Baalbaki, R., Brilke, S., Dada, L., Dias, A., Duplissy, J., El Haddad, I., Finkenzeller, H., Fischer, L.,  
153 He, X., Kim, C., Kürten, A., Lamkaddam, H., Lee, C. P., Lehtipalo, K., Leiminger, M., Manninen, H.  
154 E., Marten, R., Mentler, B., Partoll, E., Petäjä, T., Rissanen, M., Schobesberger, S., Schuchmann, S.,  
155 Simon, M., Tham, Y. J., Vazquez-Pufleau, M., Wagner, A. C., Wang, Y., Wu, Y., Xiao, M.,  
156 Baltensperger, U., Curtius, J., Flagan, R., Kirkby, J., Kulmala, M., Volkamer, R., Winkler, P. M.,  
157 Worsnop, D. and Donahue, N. M.: Molecular Composition and Volatility of Nucleated Particles from  
158  $\alpha$ -Pinene Oxidation between  $-50\text{ }^{\circ}\text{C}$  and  $+25\text{ }^{\circ}\text{C}$ , *Environ. Sci. Technol.*, 53(21), 12357–12365,  
159 doi:10.1021/acs.est.9b03265, 2019.

160